

The Neural Substrate of Spectral Preference in *Drosophila*

Shuying Gao,^{1,8} Shin-ya Takemura,^{2,8} Chun-Yuan Ting,^{1,8} Songling Huang,¹ Zhiyuan Lu,² Haojiang Luan,³ Jens Rister,^{4,9} Andreas S. Thum,⁴ Meiluen Yang,¹ Sung-Tae Hong,⁵ Jing W. Wang,⁶ Ward F. Odenwald,⁷ Benjamin H. White,³ Ian A. Meinertzhagen,^{2,*} and Chi-Hon Lee^{1,*}

¹Unit on Neuronal Connectivity, Laboratory of Gene Regulation and Development, National Institute of Child Health and Human Development, National Institutes of Health, Bethesda, MD 20892, USA

²Life Sciences Centre, Dalhousie University, Halifax, Nova Scotia B3H 4J1, Canada

³Unit on Neural Function, Laboratory of Molecular Biology, National Institute of Mental Health, National Institutes of Health, Bethesda, MD 20892, USA

⁴Lehrstuhl für Genetik und Neurobiologie, Universität Würzburg, Am Hubland, 97074 Würzburg, Germany

⁵Laboratory for Neural Network of Cognition, Department of Biological Sciences, Korea Advanced Institute of Science and Technology, Guseong-Dong, Yusong-Gu, Daejeon 305-701, Korea

⁶Division of Biological Sciences, University of California, San Diego, La Jolla, CA 92093, USA

⁷Neural Cell-Fate Determinants Section, National Institute of Neurological Disorder and Stroke, National Institutes of Health, Bethesda, MD 20892, USA

⁸These authors contributed equally to this work

⁹Present address: Center for Developmental Genetics, Department of Biology, New York University, 1009 Silver Center, 100 Washington Square East, New York, NY 10003, USA

*Correspondence: i.a.meinertzhagen@dal.ca (I.A.M.), leechih@mail.nih.gov (C.-H.L.)

DOI 10.1016/j.neuron.2008.08.010

SUMMARY

Drosophila vision is mediated by inputs from three types of photoreceptor neurons; R1–R6 mediate achromatic motion detection, while R7 and R8 constitute two chromatic channels. Neural circuits for processing chromatic information are not known. Here, we identified the first-order interneurons downstream of the chromatic channels. Serial EM revealed that small-field projection neurons Tm5 and Tm9 receive direct synaptic input from R7 and R8, respectively, and indirect input from R1–R6, qualifying them to function as color-opponent neurons. Wide-field Dm8 amacrine neurons receive input from 13–16 UV-sensing R7s and provide output to projection neurons. Using a combinatorial expression system to manipulate activity in different neuron subtypes, we determined that Dm8 neurons are necessary and sufficient for flies to exhibit phototaxis toward ultraviolet instead of green light. We propose that Dm8 sacrifices spatial resolution for sensitivity by relaying signals from multiple R7s to projection neurons, which then provide output to higher visual centers.

INTRODUCTION

Many animals respond differentially to light of different wavelengths; for example, most flying insects exhibit positive phototactic responses but prefer ultraviolet (UV) to visible light, whereas zebrafish are strongly phototactic to ultraviolet/blue

and red light but weakly to green (Menzel, 1979; Menzel and Backhaus, 1991; Orger and Baier, 2005). Unlike true color vision, which distinguishes light of different spectral compositions (hues) independently of their intensities, spectral preferences are strongly intensity dependent and innate, probably reflecting each species' ecophysiological needs. Thus, water fleas (*Daphnia magna*) avoid harmful UV but are attracted to green light, which characterizes abundant food sources (Storz and Paul, 1998). Daylight is rich in UV, so flying insects' preference for UV over visible light is probably related to the so-called open-space response, the attraction toward open, bright gaps and away from dim, closed sites (Goldsmith, 1961; Hu and Stark, 1977). The receptor mechanisms for spectral preferences have been well studied in flying insects, especially in *Drosophila* (Heisenberg and Buchner, 1977). Two or more photoreceptor types with distinct spectral responses are required to detect different wavelengths of light, and mutant flies lacking UV-sensing photoreceptors exhibit aberrant preference for green light (Hu and Stark, 1977). However, the postreceptoral mechanisms of spectral preference are entirely unknown. Furthermore, it is not clear how spectral preference is related to true color vision. Color-mixing experiments suggest that color vision and spectral preference are independent in honeybees (Menzel and Greggers, 1985). In *Drosophila*, however, spectral preference experiments have revealed that the phototactic response toward UV is significantly enhanced by the presence of visible light, suggesting a "color" contrast effect in spectral preference behavior (Schümperli, 1973; Fischbach, 1979). Identifying and characterizing the neural circuits that process chromatic information is the first step to understanding the postreceptoral mechanisms of spectral preference and, thus, color vision.

With recent advances in genetic techniques that manipulate neuronal function, *Drosophila* has re-emerged as a model

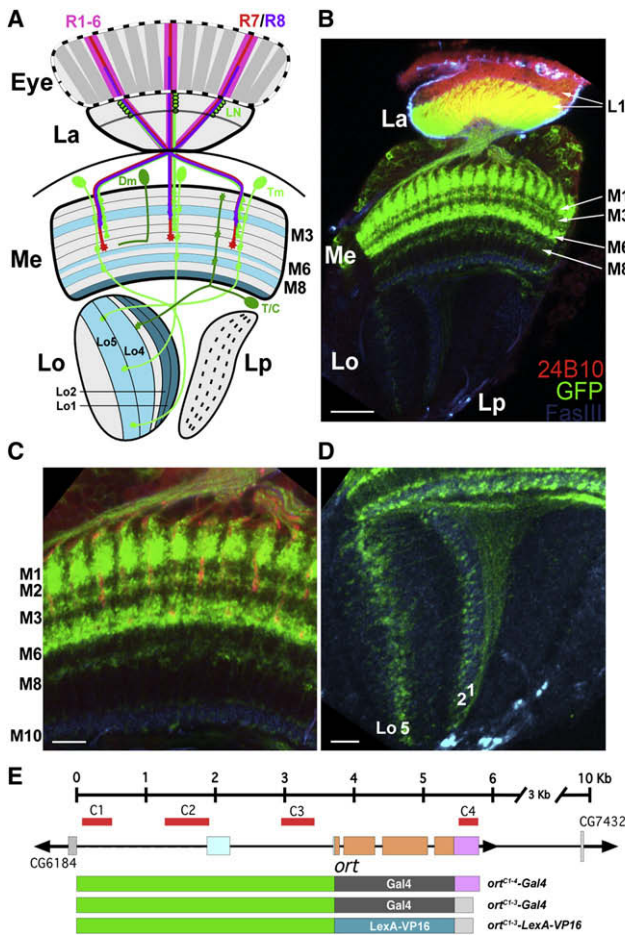


Figure 1. The Histamine Chloride Channel *Ort* Is Expressed in Subsets of Lamina and Medulla Neurons

(A) A schematic illustration of the *Drosophila* visual system, including the eye (Eye) and four optic neuropils: lamina (La), medulla (Me), lobula (Lo), and lobula plate (Lp). The outer photoreceptors, R1–R6 (pink), terminate in the lamina and synapse with lamina neurons (LN; green). The central photoreceptors, R7 (red) and R8 (purple), project axons to the medulla strata M6 and M3, respectively. Three selected types of medulla neurons are shown: transmedulla (Tm) neurons arborize in various medulla strata and project axons to distinct lobula strata, distal medulla (Dm) amacrine neurons extend processes in distal medulla strata, and T and C (T/C) neurons extend axons into the medulla and lobula (T2 neurons) or lamina (C2 neurons, data not shown). Medulla and lobula strata marked by anti-FasIII antibody are colored cyan.

(B) The *ort* promoter driver labels subsets of medulla neurons. The *ort*^{C1-3}-*LexA::VP16* driver was used to drive the expression of rCD2::GFP, a membrane-tethered GFP marker (green) in the lamina and medulla neurons that are postsynaptic to photoreceptors. Photoreceptor axons were visualized using MAb24B10 antibody (red). Anti-FasIII antibody (blue), which labels distinct medulla and lobula strata, was used as a stratum-specific landmark. (C and D) High magnification views of (B), showing the medulla (C) and lobula neuropil (D).

(D) The GFP-labeled transmedulla neurons project axons to strata Lo1, Lo2, and Lo5 of the lobula (Lo1, 2, and 5), forming a topographic map.

(E) Promoter analysis of the *ort* gene. The *ort* genomic structure shown as a linear cartoon with boxes representing exons and lines representing introns and intergenic sequences. Comparative genomic analysis identifies four blocks of sequences, C1–C4 (red, shown above the genomic structure), that are highly conserved among 12 species of *Drosophila* (see Figure S2A). The

system for studying neural circuits and functions. In particular, the Gal4/UAS expression system combined with the temperature-sensitive allele of *shibire* makes it possible to examine the behavioral consequences of reversibly inactivating specific subsets of neurons (Kitamoto, 2001). Such interventions allow direct comparisons between the connections of a neuron and its function, thereby establishing causality (reviewed in Luo et al., 2008).

The *Drosophila* visual system comprises the compound eye and four successive optic neuropils (lamina, medulla, lobula, and lobula plate; Figure 1A). The compound eye itself has some 750 ommatidia populated by two types of photoreceptors. The outer photoreceptors R1–R6, which are in many ways equivalent to vertebrate rod cells, express Rh1 opsin (O'Tousa et al., 1985), respond to a broad spectrum of light (Hardie, 1979), and are thus presumed to be achromatic. The inner photoreceptor neurons R7 and R8 have complex opsin expression patterns (reviewed in Mikeladze-Dvali et al., 2005); R7s express one of two UV-sensitive opsins, Rh3 and Rh4, while, beneath R7, the R8s coordinately express blue-sensitive Rh5 or green-sensitive Rh6 opsins (Salcedo et al., 1999). The achromatic R1–R6 channel mediates motion detection (Heisenberg and Buchner, 1977; Yamaguchi et al., 2008). R1–R6 innervate the lamina, where the achromatic channel input diverges to three or more pathways mediated by three types of lamina neurons, L1–L3. Their synaptic connections have been analyzed exhaustively at the electron microscopic (EM) level (Meinertzhagen and O'Neil, 1991; Meinertzhagen and Sorra, 2001). Genetic dissection indicates that these three pathways serve different functions in motion detection and orientation (Rister et al., 2007). Much like vertebrate cones, R7 and R8 photoreceptors are thought to constitute chromatic channels that are functionally required for spectral preference behaviors (Heisenberg and Buchner, 1977). The axons of R7 and R8 penetrate the lamina and directly innervate the distal medulla, where, until now, their synaptic connections have been completely unknown.

The medulla, the largest and most heavily populated optic neuropil, is organized into strata (M1–M10) and columns (Fischbach and Dittrich, 1989; Campos-Ortega and Strausfeld, 1972) in a manner reminiscent of the mammalian cortex. All visual information converges upon the distal strata of the medulla; the axons of R7 and R8 directly innervate strata M6 and M3, respectively, while L1–L3 transmit information from the R1–R6 channel to multiple medulla strata (M1/M5, M2, and M3, respectively). Terminals of those R7, R8, and L1–L3 that view a single point in visual space innervate a single medulla column (Meinertzhagen, 1976) and there establish a retinotopic pixel. Previous Golgi studies have revealed about 60 morphologically distinct types of medulla neurons (Fischbach and Dittrich, 1989). Each arborizes in a stereotypic pattern within specific strata of the medulla and projects an axon to a distinct stratum of the medulla, lobula, or lobula plate. The distinct morphological forms of different types

ort promoter (C1–C3) with the *ort* or *hs70* 3' UTR region (purple and gray, respectively) was fused to either the yeast transcription factor Gal4 (dark gray box) or the chimeric transcription factor LexA::VP16 (blue box) to generate various *ort* promoter drivers (as indicated). (Orange box) Coding region. (Cyan box) 5' UTR. (Purple box) 3' UTR. Scale bars: (B) 20 μ m; (C and D) 10 μ m.

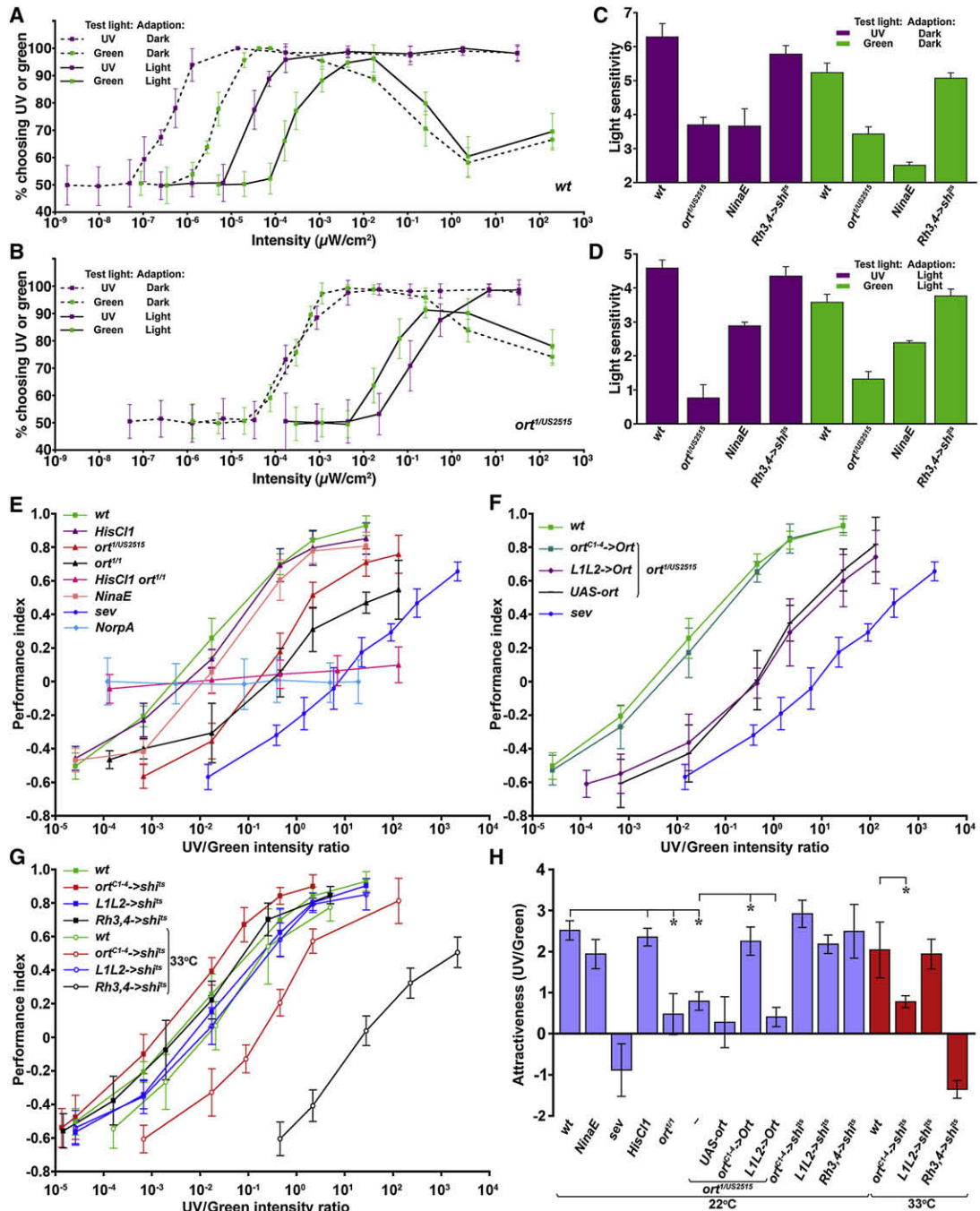


Figure 2. Ort-Expressing Neurons Mediate Phototaxis and a Normal Preference for UV

(A–D) Wild-type (A), *ort* (B), and various mutant flies were tested for fast phototaxis toward UV or green light. The intensity–response curves were measured by recording the percentage of flies choosing UV or green light of various intensities over dark. Light intensity was shown as a logarithmic scale, and error bars (standard deviations) represent the variations among trials.

(A) Wild-type flies exhibited phototactic responses to UV in a simple intensity-dependent fashion, resulting in a sigmoidal intensity–response curve. In contrast, phototactic response toward green light was not monotonous because the response was reduced at high intensities of green light. Compared with dark adaptation (dotted lines), light adaptation (solid lines) decreased sensitivity to both UV and green light by approximately two orders of magnitude.

(B) Compared with wild-type, *ort* mutants exhibited a significantly reduced phototactic response under dark- or light-adapted conditions. In *ort* mutants, phototaxis toward UV appeared to be affected more severely than that toward green light.

(C and D) Histograms of light sensitivity of wild-type and various mutant flies under dark- (C) or light-adapted (D) conditions. Light sensitivity, defined as the negative logarithm of the minimal light intensity required to attract 75% of the test flies, was calculated from the intensity–response curves. Note that fast

of medulla neurons reflect, at least in part, their diverse patterns of gene expression (Morante and Desplan, 2008). Although it is widely presumed that the medulla incorporates key neural substrates for processing color and motion information, little is known about its synaptic circuits and their functions. EM analyses of synaptic circuits have not been possible because of the complexity of this neuropil, while electrophysiological investigations are technically challenging because of the small size of neurons.

In this study, we investigate the chromatic visual circuits in the medulla. Using a combination of transgenic and histological approaches, we identify the first-order interneurons in the medulla that receive direct synaptic inputs from the chromatic channels R7 and R8. We then subdivide these neurons based on their use of neurotransmitters and gene expression patterns. By systematically inactivating and restoring the activity of specific neuron subtypes, we identify the neurons that are necessary and sufficient to drive a fly's phototactic preference to UV.

RESULTS

The Histamine Chloride Channel *Ort* Is Required for UV/Green Spectral Preference

Previous electrophysiological and histological studies have demonstrated that *Drosophila* photoreceptor neurons are histaminergic (Hardie, 1987; Sarthy, 1991) and that R7 and R8 photoreceptors provide the predominant histamine-immunoreactive input to the medulla (Pollack and Hofbauer, 1991). Two ionotropic histamine-gated channels, *Ort* (ora transientless; *HisCl2*) and *HisCl1*, have been identified (Gengs et al., 2002; Gisselmann et al., 2002; Zheng et al., 2002; Witte et al., 2002; Pantazis et al., 2008). Mutants for *ort* exhibit defects in motion detection and their electroretinograms (ERGs), indicating that *Ort* is required to transmit R1–R6 input to the first-order interneurons (Gengs et al., 2002). To test whether *Ort* is required for visually guided behavior, we first examined flies' phototaxis toward either UV or green light in preference to dark (see Experimental Procedures for details). This phototactic response is mediated primar-

ily by the more sensitive, broad-spectrum photoreceptors, R1–R6, although R7 cells also contribute to UV, but not green, phototaxis under the light-adapted condition (Figures 2C and 2D, and Figures S1A and S1B available online; Fischbach, 1979). We found that wild-type flies exhibited stronger phototaxis toward UV than toward green light by approximately one order of magnitude and that light adaptation, when compared with dark adaptation, reduced the sensitivity to UV and green light by approximately two orders of magnitude (Figure 2A). In contrast, strong transallelic combination *ort*¹/*ort*^{US2515} mutant flies exhibited much weaker phototaxis toward either UV or green light (by about three and two orders of magnitude, respectively) as compared with wild-type. In negative geotaxis assays, *ort* mutants exhibited no apparent motor defects (Figure S1C), suggesting that their reduced phototaxis was not a motor system defect but rather a visual deficit. In addition, the *ort* mutation affected UV phototaxis more severely than green phototaxis. We speculate that *Ort* plays a role in relaying signals from UV-sensing R7s to their first-order interneurons and that *HisCl1* may participate in phototaxis, especially toward green light.

To assess whether *Ort* is required to transmit chromatic input mediated by R7 and R8, we used a quantitative spectral preference assay. This spectral preference assay tests the phototaxis toward UV in preference to green (see Experimental Procedures for details) and depends on R7, but not significantly on R1–R6, function (Figures 2E and 2G; Jacob et al., 1977; Fischbach, 1979). This behavior depends on the circuit comparing UV and green light and likely reflects salience of UV and green lights rather than a simple linear summation of their phototactic responses. We found that wild-type flies preferred short-wavelength UV to longer-wavelength green light in an intensity-dependent fashion (Figure 2E). In contrast, homozygous null *ort*¹ mutants and strong transallelic combination *ort*¹/*ort*^{US2515} mutants (as well as other allelic combinations *ort*^{P306}/*ort*^{US2515} and *ort*¹/*ort*^{P306}; data not shown) all exhibited reduced UV preference. Over five orders of magnitude in the ratio of UV/green intensities, the proportion of *ort* mutant flies that chose UV was significantly lower than that for wild-type flies (Figure 2E).

phototaxis toward UV or green light was driven primarily by the broad-spectrum R1–R6 photoreceptors since this behavior was significantly affected by the inactivation of R1–R6 (*NinaE* mutants), but not R7 cells (*Rh3,4- > shi^{ts1}*).

(E–H) Wild-type, *ort*, *HisCl1*, and various mutant flies tested for phototactic preference to UV over green light. The intensity-response curves were measured by varying UV intensity while keeping the green light intensity constant (see Experimental Procedures for details). (E–G) The P.I. for each genotype was calculated from the numbers of flies choosing UV (N_{UV}) or green (N_G) light by the following formula: $P.I. = [N_{UV} - N_G] / [N_{UV} + N_G]$. The UV/green intensity ratio (E–G) is shown as a logarithmic scale. Error bars (standard deviations) represent the variations among trials.

(E) *ort* mutants had a reduced preference for UV. Wild-type (*wt*) flies exhibited phototactic preference to UV in an intensity-dependent fashion, resulting in a sigmoidal intensity-response curve. For *ort* mutants (*ort*^{1/1} and *ort*^{1/US2515}), the intensity-response curve was shifted to the right. Note that normal UV preference requires R7s, but not R1–R6, as *sevenless* (*sev*^{E2}) mutants, but not *NinaE* mutants, exhibited low UV preference. *HisCl1 ort* double-null mutants, like *norPA*⁹⁶, a phototransduction mutant, chose UV and green light indiscriminately over a broad range of UV/green intensity ratios.

(F) The expression of *Ort* driven by *ort*^{CT-4}-*Gal4* restored normal UV preference in *ort* mutants. In contrast, *UAS-ort* alone or reinstating *Ort* function in the achromatic channels L1 and L2 failed to restore UV preference in *ort* mutants. Positive control (*wt*) and negative control (*sev*) were from those described in (E). (G) *Ort*-expressing neurons are required for normal UV preference. *Shi*^{ts1} expressed in *Ort*-expressing neurons or R7s blocks their synaptic transmission. At a restrictive temperature (33°C), *ort*^{CT-4}- *> shi^{ts1}* flies exhibited lower UV preference compared with wild-type controls. Inactivating R7s using *Rh3,4- > shi^{ts1}* resulted in an even greater reduction in UV preference. In contrast, inactivating L1 and L2 using *L1L2- > shi^{ts1}* did not affect UV preference. Wild-type control (*wt*) at 22°C was from that described in (E).

(H) Histogram of the relative attractiveness of UV over green light ($Attr_{UV/G}$) for each genotype. $Attr_{UV/G}$ was calculated from the UV/green intensity ratio at which flies exhibited phototaxis to UV and green lights with equal frequency (isoluminance point, P.I. = 0), based on the following formula: $Attr_{UV/G} = -\log(UV/green \text{ ratio at the isoluminance point})$. The difference between the $Attr_{UV/G}$ of the wild-type and *ort* mutants (*ort*^{CT-4}- *> shi^{ts1}* flies) was statistically significant ($p < 0.00001$), whereas the difference between the wild-type and rescued *ort* mutants (*ort HisCl1* mutants) was not ($p > 0.1$).

To quantify the UV preference, we determined the isoluminance point, the UV/green intensity ratio at which flies found light of either wavelength equally “attractive,” and used the negative logarithm of the intensity ratio as a measure of UV attractiveness ($\text{Attr}_{\text{UV/G}}$; Figure 2H). The UV attractiveness for *ort* mutants ($\text{Attr}_{\text{UV/G}} = 0.47 \pm 0.50$ for *ort*¹ and 0.79 ± 0.22 for *ort*¹/*ort*^{US2515}; mean \pm SD) was significantly lower than that for wild-type flies ($\text{Attr}_{\text{UV/G}} = 2.52 \pm 0.23$) but higher than that for *sevenless* mutants ($\text{Attr}_{\text{UV/G}} = -0.88 \pm 0.64$), which lack UV-sensing R7s entirely (Tomlinson and Ready, 1986) ($p < 0.00001$, Student's *t* test; Figures 2E and 2H).

Given that *ort* null mutants still exhibited phototaxis, we examined whether the other histamine receptor, HisCl1, might have contributed to UV preference. We found that *HisCl1*¹³⁴ null mutants exhibited UV preference indistinguishable from the wild-type ($p > 0.1$). In contrast, strong allelic combination *HisCl1*¹³⁴ *ort*¹/*HisCl1*¹³⁴ *ort*^{P306} double mutants showed weak phototaxis toward green light (data not shown), while double-null *HisCl1*¹³⁴ *ort*¹ mutants, like the phototransduction mutant *NorpA*, failed to discriminate between wavelengths in the UV and green (Figure 2E). We conclude that Ort is essential for optimal UV preference, while HisCl1 plays, at most, a minor and partially redundant role. We note that double-null *HisCl1*¹³⁴ *ort*¹ mutants were not entirely blind and still exhibited very weak fast phototaxis (data not shown), suggesting that there might be residual synaptic transmission between photoreceptors and the first-order interneurons despite the absence of these two known histamine receptors.

The Histamine Chloride Channel Ort Is Expressed in Subsets of Lamina and Medulla Neurons

We reasoned that the first-order interneurons must express the histamine receptor Ort in order to respond to their inputs from histaminergic R7 and R8 terminals. To identify these first-order interneurons, we determined the *ort* promoter region using comparative genomic sequence analysis (Odenwald et al., 2005). In the *ort* locus, we found four blocks of noncoding sequence that are highly conserved among 12 species of *Drosophila* (Figure S2A). The first three sequence blocks (designated C1–C3) are localized to the intergenic region and the first intron and are, therefore, likely to contain critical *cis* elements (Figures 1E and S2A). We generated *ort*-promoter constructs driving Gal4 or LexA::VP16, designating these *ort*^{C1-3}-Gal4 and *ort*^{C1-3}-LexA::VP16. Both driver systems drove expression patterns in identical subsets of neurons in the lamina, medulla cortices, and in the deep C and T neurons of the lobula complex (Figures 1B–1D), except that *ort*^{C1-3}-Gal4 drove somewhat patchy expression with lower intensity (data not shown). The fourth block of conserved sequences, located at 3'UTR, contains putative microRNA-binding sites (Figure S2A) and, as examined in *ort*^{C1-4}-Gal4, did not drive expression in additional cells (data not shown), suggesting that it does not contain critical *cis* elements. Overall, the expression patterns of these *ort* promoter constructs resembled previously published *ort* expression patterns from *in situ* hybridization (Witte et al., 2002).

We also performed comparative genomic sequence analysis for the *HisCl1* locus and identified two blocks of highly conserved

sequence (C1 and C2), located in the first introns of the *HisCl1* gene and its neighboring gene (CG17360) (Figure S2B). We generated a *HisCl1-Gal4* construct that included these conserved sequences (Figure S3A). We found that HisCl1-Gal4 drove strong expression in the lamina epithelial glia cells (as recently also reported by Pantazis et al., 2008) and in medulla cells that are not well characterized (Figures S3B–S3D). This result is consistent with previous EM data that lamina epithelial glia envelop each cartridge and are postsynaptic to R1–R6 (Meinertzhagen and O'Neil, 1991). Insofar as both the behavioral requirement and expression pattern indicate that Ort, but not HisCl1, plays a critical role in the visual system, we focused on Ort in the following analyses.

Ort-Expressing Neurons Are Required for Visually Driven Behaviors

We next examined whether using the *ort*-promoter Gal4 drivers to express Ort was sufficient to rescue the visual behavioral defects in *ort* mutants. We found that *ort*^{C1-4}-Gal4-driven Ort expression restored a preference for UV ($\text{Attr}_{\text{UV/G}} = 2.25 \pm 0.34$) in *ort* mutants to the wild-type level (2.52 ± 0.23 ; Figures 2F and 2H). Since Ort, but not HisCl1, is also required in lamina neurons for normal ERG and motion detection responses (Figures S4B and S4C; Gengs et al., 2002; Rister et al., 2007), we examined the rescued flies for these functions too. We found that expressing Ort in *ort* mutants using *ort*^{C1-3}-Gal4 restored, at least qualitatively, the “on” and “off” transients of the ERG, which report transmission in the lamina (Coombe and Heisenberg, 1986), as well as the optomotor behavior (Figures S4B–S4D). These findings are consistent with the observation that *ort-Gal4* drove reporter expression in lamina neurons L1–L3 (Figure S4A). In contrast, expressing Ort in lamina neurons L1 and L2 using an L1/L2-specific driver (*L1L2-A-Gal4*) rescued both the ERG, at least qualitatively, and optomotor defects (Figures S4B and S4D), but not the UV preference ($\text{Attr}_{\text{UV/G}} = 0.41 \pm 0.23$; Figures 2F and 2H), of *ort* mutants. Thus, the actions of the *ort-Gal4* drivers recapitulated the endogenous Ort expression pattern in the first-order interneurons of R1–R6 and R7.

We next examined whether the Ort-expressing neurons were required for UV preference and motion detection. We found that *ort*^{C1-4}-Gal4 or *ort*^{C1-3}-LexA::VP16 driving a temperature-sensitive allele of *shibire*, *shi*^{ts1}, so as to block synaptic transmission in specific neurons (Kitamoto, 2001), significantly reduced the UV attractiveness at nonpermissive, but not permissive, temperatures ($\text{Attr}_{\text{UV/G}} = 0.78 \pm 0.14$ at 33°C and 2.92 ± 0.33 at 22°C for *ort*^{C1-4}; Figures 2G and 2H; $\text{Attr}_{\text{UV/G}} = 0.65 \pm 0.20$ at 33°C and 2.22 ± 0.40 for *ort*^{C1-3}; data not shown; $p < 0.0001$). This reduction was smaller than that caused by inactivating the R7s alone ($\text{Attr}_{\text{UV/G}} = -1.36 \pm 0.22$ at 33°C and 2.49 ± 0.65 at 22°C; Figures 2G and 2H). These results suggest that Ort-expressing neurons might mediate both UV and green phototaxis, presumably by relaying R7 and R8 channel signals, although we cannot rule out the existence of an *ort*-independent UV-sensing pathway (see Figure 5 and Discussion). Similarly, inactivating Ort-expressing neurons abolished the flies' ability to detect motion (Figure S4D). Thus, we may conclude that Ort-expressing neurons are required for both spectral preference and motion detection.

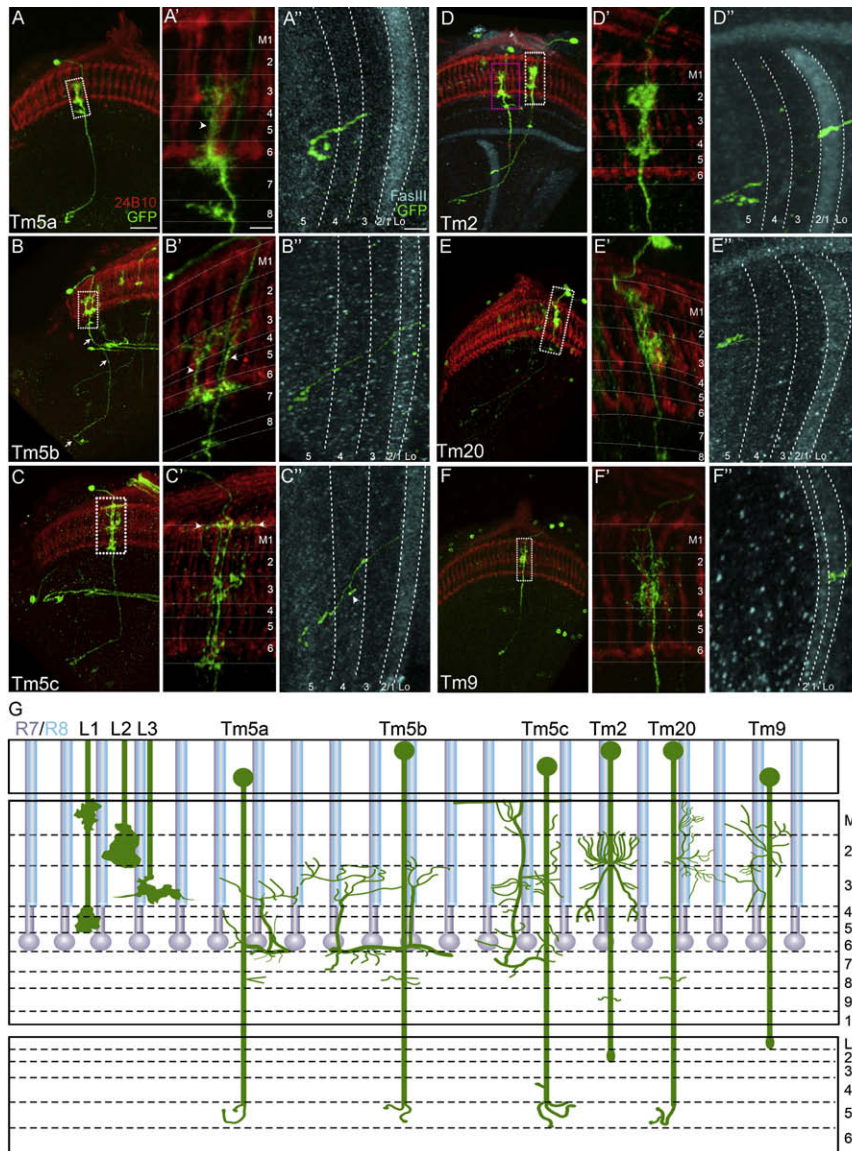


Figure 3. Orx Is Expressed in Subsets of Transmedulla Neurons

Axonal and dendritic projections (green) of single Orx-expressing transmedulla neurons were examined in flies carrying *ort^{C1-3}-Gal4*, *hs-Flp*, and *UAS > CD2, y+ > CD8-GFP* transgenes. R7 and R8 photoreceptor axons, visualized with MAb24B10 antibody (red), served as landmarks for medulla columns. Medulla and lobula strata were identified using R7 and R8 terminals and anti-FasIII immunolabeling (cyan; see Figure S5). Four Tm types, including Tm5, Tm2, Tm20, and Tm9, were identified based on their dendritic morphologies (A'–F') and stratum-specific axon terminations (A''–F''). Tm5 was further categorized into three subtypes: Tm5a, b, and c (A–C; see text for details).

(A–A'') The Tm5a neuron extends a single main dendritic branch (arrowhead), which runs along the photoreceptor terminals and extends multiple fine processes in strata M3 and M6 (A'). Its axon terminal in the Lo5 stratum is hook shaped (A'').

(B–B'') The Tm5b neuron extends two or three main dendritic branches (arrowheads) with fine processes spanning approximately five columns in strata M3, M6, and also M8 (B'); its axon terminates in stratum Lo5 (B'').

(C–C'') The Tm5c neuron extends a single main dendritic branch with multiple fine processes, which span multiple columns in strata M3 and M6. The most distinctive features of Tm5c are the dendritic arbors in the superficial part of the M1 stratum (arrowhead, C') and the presence of axon terminals (arrowhead, C'') in both strata Lo4 and Lo5.

(D–D'') Tm2 (D–D''), Tm20 (E–E''), and Tm9 (F–F'') form type-specific dendritic arbors largely confined to a single medulla column and project their axons to specific lobula strata.

(A'–F', A''–F'') High-magnification views of (A–F) in the medulla (A'–F') and lobula (A''–F''), respectively. Scale bars: 20 μ m in (A) for (A)–(F); 5 μ m in (A') for (A')–(F'); 5 μ m in (A'') for (A'')–(F'').

(G) Schematic diagram illustrating the dendritic and axonal morphologies of Tm neurons. All are shown in dorsoventral view (as in [A]–[F'']) except Tm2, which is in approximately mediolateral view.

Orx Is Expressed in a Subset of Projection Neurons in the Medulla

To identify the Orx-expressing neurons that could be synaptic targets of the R7 and R8 channels, we employed a single-cell mosaic technique based on the flip-out genetic method previously described (Wong et al., 2002). In this system, we used the *ort^{C1-3}-Gal4* flies that also carried the transgenes *UAS > CD2, y+ > CD8-GFP* and *hs-Flp*. The flipase activity induced by brief heat-shock at the second- or third-instar larval stages excited the FLP-out cassette in small random populations of cells, thereby allowing Gal4 to drive the expression of the CD8-GFP marker. From more than 1000 brain samples, we examined 459 clones of transmedulla neurons, the projection neurons that arborize in the medulla and project axons to the lobula. To identify the exact medulla and lobula strata in which these processes extended, we screened expression patterns of a series of known

cell-adhesion molecules and found three useful stratum-specific markers, FasIII, Connectin, and Capricious (Figure S5; Shinza-Kameda et al., 2006). In particular, anti-FasIII immunolabeled medulla and lobula strata of interest and, with MAb24B10 immunolabeling, was used primarily to identify the medulla and lobula strata. Based on the morphologies and stratum-specific locations of the arborization and axon terminals, we could readily assign four types of Orx-expressing projection neurons to types previously described from Golgi impregnation (Fischbach and Dittrich, 1989). These were Tm2, Tm5, Tm9, and Tm20 (Figure 3). In addition, the *ort*-promoter driver labeled, albeit at a lower frequency, centrifugal neurons C2 and T2, and three types of medulla intrinsic neurons, Dm8, other amacrine-like, and also glia-like cells (Figures 7 and S6). All of these cells were identified multiple times in at least two independent *ort-Gal4* lines, but, given the sampling nature of the single-cell mosaic technique,

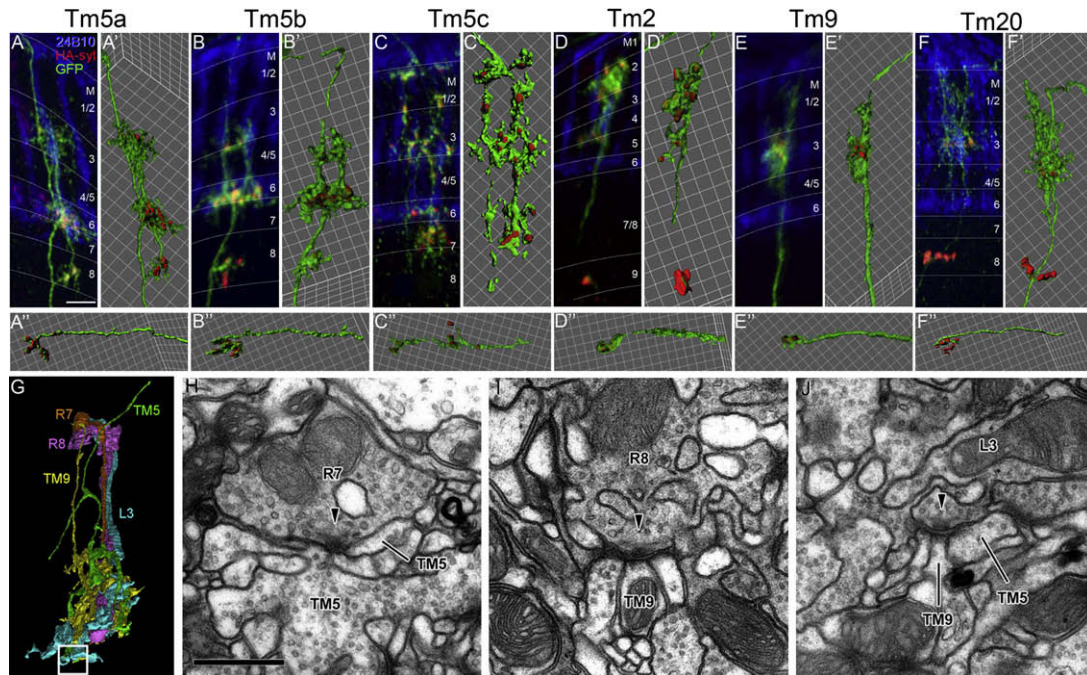


Figure 4. Ort-Expressing Tm Neurons Receive Multichannel Inputs in the Medulla and Are Presynaptic at Both the Medulla and Lobula
 (A–F) The distribution of presynaptic terminals of single Ort-expressing Tm neurons was examined in flies carrying *ort^{C1-3}-Gal4*, *hs-Flp*, *TubP* > *Gal80* >, *UAS-mCD8GFP* (green), and *UAS-synaptotagmin-HA* (red). Localization of the presynaptic reporter, synaptotagmin-HA, was visualized using anti-HA antibody. R7 and R8 photoreceptors were visualized using MAb24B10 antibody (blue). Tm cell types are as indicated. IsoSurface representations of medulla arborization (A'–F') and lobula terminals (A''–F'') were generated using Imaris software. Synaptotagmin-HA was localized to the tips of the axon terminals and dendritic arbors, the latter especially in the proximal medulla strata (M7 for Tm5c; M8 for Tm5a, Tm5b, and Tm20; M9 for Tm2).
 (G) Profiles of R7, R8, L3, Tm5, and Tm9 reconstructed in three dimensions from a single medulla column. The white square box indicates the contact site between L3 and both Tm5 and Tm9 shown in (J). Although the partially reconstructed profile resembles Tm5a, the subtype reconstructed is still not certain.
 (H–J) Synaptic contacts between R7 and Tm5 (H), R8 and Tm9 (I), and L3 and both Tm9 and Tm5 (J). Arrowheads point to T-bar ribbons in presynaptic elements, in the presumed direction of transmission.
 Scale bars: 5 μ m in (A) for (A)–(F); 500 nm in (H) for (H)–(J).

we cannot exclude the possibility that we might have missed some very rare Ort-expressing neurons. The amacrine-like and glia-like cells had not been previously described from Golgi impregnation (Fischbach and Dittrich, 1989), suggesting that there are even more classes of medulla cell types than those previously reported.

The Ort-expressing Tm neurons exhibited type-specific patterns of arborization and axon projection. Tm5 neurons extended dendrite-like processes in medulla strata M3 and M6, where R8/L3 and R7 axons terminated, respectively, and they projected axons to terminate in stratum Lo5 in the lobula. This pattern suggests that they relay information from the R7 and R8 or L3 channels to the lobula. The Tm5 neurons could be readily divided into three subtypes, Tm5a, b, and c, based on their unique dendritic patterns (see Figures 3A–3C''), the spread of their medulla arborization, and their gene expression patterns. Tm5a (n = 125) and Tm5b (n = 44) had medulla arborizations of different sizes and shapes (Figures 3A–3B'' and 3G), whereas Tm5c (n = 20) had dendritic processes in M1, in addition to strata M3 and M5, and the axon projected to both the Lo4 and Lo5 strata. The distinct morphology of Tm5c correlated with its unique expression of the vesicular glutamate transporter (see below). Tm9 (n = 43) and Tm20 (n = 67) extended type-specific

dendrite-like processes in strata M1–M3 and projected axons to distinct lobula strata (Figures 3E–3F'' and 3G). Tm20, like Tm5, projected to Lo5 while Tm9 projected to Lo1, suggesting that Tm9 and Tm20 relay information from R8 and (via lamina neurons) R1–R6 to different strata of the lobula (Figures 3E–3F'' and 3G). In medulla strata M1–M3, Tm2 (n = 160) extended dendrite-like processes that did not appear to make significant contacts with R7 or R8 terminals (Figures 3D–3D'' and 3G).

Tm Projection Neurons Relay Both Chromatic and Achromatic Channel Information to the Proximal Medulla and the Lobula

To determine whether the Ort-expressing Tm neurons indeed received synaptic input from photoreceptors, we undertook serial EM reconstructions of Tm9 (two cells), Tm2 (five cells), and parts of a single Tm5 cell that resembled Tm5a, as well as the afferent input terminals that innervate the medulla, including R7, R8, and L1–L5 (Figure 4G; Takemura et al., 2008). The fine dendritic arbor of Tm20 has so far eluded reconstruction. We found that Tm9 received direct synaptic contacts from both R8 and L3 (Figures 4I and 4J), and the Tm5 received direct synaptic contacts from R7 and L3 (Figures 4H and 4J). Thus, Tm9 and Tm5 cells were postsynaptic to both the chromatic channels

and an achromatic channel. Tm2, by contrast, received synaptic contacts from L2 and L4, but not, despite its Ort expression, R7 or R8 (data not shown). However, we cannot exclude the possibility that Tm2 responds to paracrine release of histamine from the R8 terminal or an unidentified histamine input in the lobula.

To determine whether Tm neurons could relay information from the medulla to the lobula, we localized a marker for presynaptic sites to the Tm neurons using a flipase-based genetic mosaic method. In this system, heat-shock induced expression of flipase, which, in turn, removed the Gal80, allowing the *ort-Gal4* to drive expression of a presynaptic marker, a HA-tagged synaptotagmin (*syt*-HA), and the mCD8-GFP marker in a small number of neurons. We found, as expected, that in all Ort-expressing Tm neurons, *syt*-HA was localized to the axon terminals in the lobula, indicating that these Tm neurons are qualified to be presynaptic in this neuropil (Figures 4A''–4F''). Surprisingly, we observed that *syt*-HA was also localized to the dendrite-like processes in the medulla, especially in strata M7–M10, suggesting that many of these processes contain not only post- but also presynaptic sites (Figures 4A–4F'). Especially, the processes of Tm5a, Tm5b, and Tm20 in stratum M8 were heavily decorated with *syt*-HA, suggesting that this stratum might be a significant output layer for these neurons (Figures 4A', 4B', and 4F').

Subcategorization of Ort-Expressing Neurons Based on Neurotransmitter Usage

We reasoned that Ort-expressing neurons might be divided into several groups based on their differential release of other neurotransmitters. To test this possibility, we used a series of promoter-Gal4 and enhancer trap lines driving the CD8 marker to label neurons with glutamatergic, cholinergic, GABAergic, serotonergic, and dopaminergic phenotypes in the medulla (see [Experimental Procedures](#) for details). To determine whether these neurons also express Ort, and are thus likely to receive histaminergic input, we expressed in the same animals the rCD2::GFP marker using the *ort^{C1-3}-LexA::VP16* driver (Figures S7A–S7C''). By overlaying two expression patterns, we found that many Ort-expressing neurons also expressed cholinergic or glutamatergic markers, while few did so for a GABAergic (Figure S7C–S7C'') and none appeared to do so for serotonergic or dopaminergic phenotypes (Figures S7D and S7E). In particular, we found that a group of neurons labeled by both the vesicular glutamate transporter (*vGlut^{OK371}*) and *ort-Gal4* drivers extended processes in the M6 stratum where R7 axons terminate, suggesting that R7's target neurons might be glutamatergic (Figures S7A–S7A'').

To identify candidate R7 target neurons, we employed a combinatorial gene expression system, the Split-Gal4 system (Luan et al., 2006), to restrict Gal4 activity to glutamatergic Ort-expressing neurons. In this system, *ort* and *vGlut* promoters drive expression of the Gal4DBD (Gal4 DNA-binding domain-leucine zipper) and dVP16AD (a codon-optimized VP16 transactivation domain-leucine zipper), respectively. Thus, Gal4 activity was reconstituted only in the neurons that expressed both Ort and *vGlut*. We generated a dVP16AD enhancer trap vector and substituted it for the Gal4 enhancer trap in the *vGlut* locus (see [Experimental Procedures](#) for details). The resulting hemidriver, *vGlut^{OK371}-dVP16AD*, in combination with a general neuronal

hemidriver, *elav-Gal4DBD*, drove expression in a pattern essentially identical to that driven by *vGlut^{OK371}-Gal4*, indicating that the *vGlut^{OK371}-dVP16AD* enhancer trap recapitulated the expression pattern of the *vGlut^{OK371}-Gal4* driver (data not shown). The combination of the *vGlut^{OK371}-dVP16AD* and *ort^{C1-3}-Gal4DBD* hemidrivers (designated *ort^{C1-3}∩vGlut*) gave rise to expression in a subset of Ort-expressing neurons in the optic lobe, namely those that express a glutamate phenotype and are thus likely to be glutamatergic (Figure 5A). Single-cell mosaic analysis (using *hs-Flp* and *UAS > CD2 > mCD8GFP*) revealed that the combinatorial *ort^{C1-3}∩vGlut* driver was expressed in Dm8, Tm5c, and L1 neurons, as well as in the medulla glia-like cells (data not shown). In contrast, *cha∩ort^{C1-3}*, the combination of *cha-Gal4DBD* (choline acetyltransferase-Gal4DBD) and *ort^{C1-3}-Gal4AD* hemidrivers drove expression in the Ort-expressing neurons that expressed a cholinergic phenotype (Figure 5B), including L2, Tm2, Tm9, and Tm20 (data not shown). Notable among these findings, L1 and L2, paired lamina neurons that receive closely matched R1–R6 input in the lamina, express different neurotransmitter phenotypes (L1: glutamate; L2: acetylcholine).

The Amacrine Dm8 Neuron Is Both Necessary and Sufficient for Optimal UV Preference

To determine whether glutamatergic Ort-expressing neurons confer UV preference in flies, we examined whether expressing Ort in these neurons is sufficient to restore normal UV preference in *ort* mutants. We found that expressing Ort using the combinatorial *ort^{C1-3}∩vGlut* driver restored normal UV preference in *ort* mutants ($\text{Attr}_{\text{UV/G}} = 2.26 \pm 0.30$) (Figures 5C and 5D). In contrast, expressing Ort in cholinergic Ort-expressing neurons using the *cha∩ort^{C1-3}* driver further reduced UV preference ($\text{Attr}_{\text{UV/G}} = -0.79 \pm 0.21$), suggesting that the cholinergic Ort-expressing neurons reduce UV attraction or, more likely, enhance green attraction (Figures 5C and 5D). Although the *cha∩ort^{C1-3}* and *ort^{C1-3}∩vGlut* drivers were expressed in specific subsets of Ort-expressing neurons in the optic lobe, they showed additional expression outside the visual system, and expressing *sh¹ts1* with either driver caused nonspecific motor defects at the nonpermissive temperature (data not shown). Although we could not test whether the glutamatergic Ort-expressing neurons were required for UV preference, our rescue results indicated that the candidate glutamatergic Ort-expressing neurons, which included Dm8 and Tm5c, were involved in UV preference.

To distinguish whether Dm8 or Tm5c is required for UV preference, we dissected the *ort* promoter and generated three promoter-Gal4 lines, each of which contained one of the three highly conserved regions (C1–C3) of the *ort* promoter (Figure 6A). We found that the second and third conserved regions (C2 and C3) gave rise to the expression in two different subsets of Ort-expressing neurons (Figures 6B and 6C), while C1 alone gave no detectable expression (data not shown). Using single-cell analysis, we found that *ort^{C2}-Gal4* drove expression in Dm8 and L1–L3, but not in any Tm neurons, while *ort^{C3}-Gal4* was expressed in L2, Tm2, Tm9, C2, and Mi1 neurons (data not shown). All of these neurons except Mi1 expressed Ort, suggesting that the C2 and C3 fragments of the *ort* promoter drove expression in distinct subsets of the Ort-expressing neurons

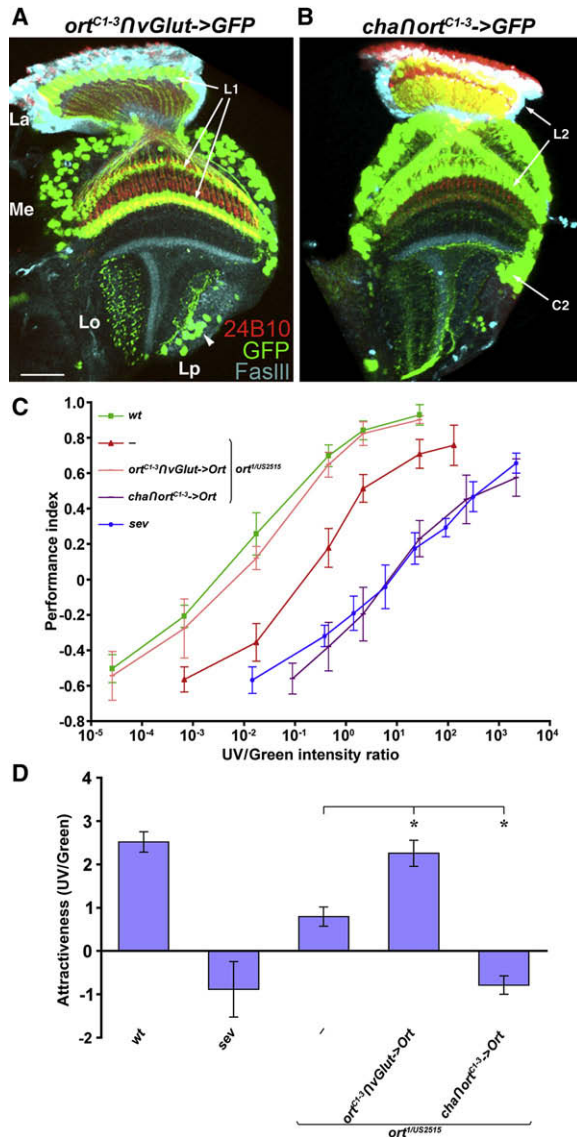


Figure 5. Glutamatergic and Cholinergic Ort-Expressing Neurons Confer UV and Green Preference, Respectively

(A and B) The combinatorial drivers, *ort^{C1-3}∩vGlut* (A) and *cha∩ort^{C1-3}* (B), are expressed in distinct neuron subsets in the adult optic lobe. The *ort^{C1-3}∩vGlut* and *cha∩ort^{C1-3}* drivers express the EGFP marker (green) in those Ort-expressing neurons with either a glutamatergic or cholinergic phenotype. The *ort^{C1-3}∩vGlut* driver labeled L1, Tm5c, and Dm8 neurons, while the *cha∩ort^{C1-3}* driver was expressed in L2, C2, Tm2, Tm9, and Tm20. Lobula plate neurons (arrowhead, A), which do not normally express Ort, were also labeled by the combinatorial drivers. (Red) Photoreceptor axons visualized with MAb24B10 antibody. (Cyan) Specific neuropil strata marked with FasIII antibody. Scale bar, 20 μ m in (A) and (B).

(C and D) Sufficiency of glutamatergic or cholinergic Ort-expressing neurons for UV and green light preference. Restoring Ort function in phenotypically glutamatergic Ort-expressing neurons (*ort^{C1-3}∩vGlut->Ort*) rescued the UV phototactic defects in *ort* mutant flies, while restoring phenotypically cholinergic Ort-expressing neurons (*cha∩ort^{C1-3}->Ort*) rendered a stronger green preference.

(C) Intensity-response curves for UV/green spectral preference were measured as described in Figure 2. *ort^{1/US2515}*, wild-type, and negative control

but that the combination of all conserved regions was required to suppress Ort expression in Mi1.

We next examined whether the *ort^{C2}* or *ort^{C3}* neuron subsets were sufficient and/or required for UV preference. We found that expressing Ort using the *ort^{C2}-Gal4* driver in *ort* mutants was sufficient to restore UV preference at least up to the wild-type level ($\text{Attr}_{\text{UV/G}} = 3.23 \pm 0.26$; Figures 6E and 6H). Because the lamina neurons L1 and L2 are neither necessary nor sufficient for UV preference (Figures 2F–2H), this finding suggested that the Dm8 neurons alone are sufficient to drive a fly's normal preference for UV. Conversely, we tested whether these neurons were required for UV preference using *shi^{ts1}*. We found that flies carrying *ort^{C2}->shi^{ts1}* exhibited strongly attenuated UV preference at the nonpermissive, but not permissive, temperatures ($\text{Attr}_{\text{UV/G}} = -1.00 \pm 0.12$ at 33°C and 1.93 ± 0.25 at 22°C; Figures 6F and 6H), indicating that the *ort^{C2}* subset is required for normal UV preference. In contrast, restoring the *ort^{C3}* subset activity further reduced UV preference ($\text{Attr}_{\text{UV/G}} = -0.84 \pm 0.44$), suggesting that the *ort^{C3}* subset inhibits UV sensing or enhances green-sensing pathways. Moreover, blocking the activity of the *ort^{C3}* subset using *shi^{ts1}* did not confer a stronger UV preference ($\text{Attr}_{\text{UV/G}} = 1.74 \pm 0.27$ at 33°C and 2.4 ± 0.31 at 22°C), suggesting that the *ort^{C3}* subset is sufficient, but likely not required, for phototactic preference to green light (Figures 6F and 6H).

The preceding evidence indicated that the two lines, *ort^{C2}* and *ort∩vGlut*, together identified the Dm8 neurons both functionally and anatomically as a substrate for UV preference. To test this possibility directly, we generated an *ort^{C2}-Gal4^{DBD}* hemidriver and combined it with the *vGlut-dVP16AD* hemidriver. We found that the combinatorial driver *ort^{C2}∩vGlut* was expressed in most Dm8 neurons, as well as in a small number of L1 neurons and glia-like cells (Figure 6D). Restoring the expression of Ort in Dm8 in *ort* or *HisCl1 ort* double-null mutants completely restored normal UV preference ($\text{Attr}_{\text{UV/G}} = 3.02 \pm 0.47$ and 2.51 ± 0.18 , respectively). Conversely, flies carrying *ort^{C2}∩vGlut->shi^{ts1}* exhibited reduced UV preference at the nonpermissive, but not permissive, temperature ($\text{Attr}_{\text{UV/G}} = -0.17 \pm 0.44$ at 33°C and 1.74 ± 0.28 at 22°C; Figures 6G and 6H). Thus, the Dm8 cells are necessary and sufficient for a fly's normal preference for UV.

Amacrine Neuron Dm8 Receives Direct Synaptic Input from Multiple R7s

Finally, using the single-cell mosaic method, we examined the morphology of the Dm8 neurons (Figures 7A and 7A'). We found that, in stratum M6, the Dm8 neurons extended web-like processes, which extensively overlapped 13–16 R7 terminals (average 14.6 ± 0.99 , $n = 15$, mean \pm SD; Figures 7A and 7A'). To determine whether Dm8 receives direct synaptic input from R7, we expressed an EM marker, HRP-CD2, in the Dm8 neurons

sev are from those described in Figure 2E. Error bars (standard deviations) represent the variations among trials.

(D) Histogram of the relative attractiveness of UV over green light ($\text{Attr}_{\text{UV/G}}$) calculated from (C). The differences between *ort* mutants and those rescued with *ort^{C1-3}∩vGlut->Ort* (and *cha∩ort^{C1-3}->Ort*) are highly significant ($p < 0.00001$). Error bars indicate SD. *ort^{1/US2515}*, wild-type, and negative control *sev* data are from those reported in Figure 2E.

using the *ort^{C2}-Gal4* driver and examined their synaptic structure at the EM level (Figure 7C). We found that most R7 synapses are triads and that Dm8 contributes to at least one of the three postsynaptic elements in essentially all R7 synapses. Cumulatively, Dm8 contributes to ~38% (18 out of 47 identified) of the elements postsynaptic to R7s, suggesting that Dm8 is a major synaptic target for these photoreceptors. In addition, we reconstructed processes of three Dm8 neurons spanning seven medulla columns. We found that Dm8 processes tiled the M6 stratum with partial overlapping so that each R7 terminal was presynaptic to one or two Dm8 neurons (Figure 7D). Examining the presynaptic structures of the Dm8 neurons at EM and light microscopic levels revealed that the Dm8 neurons were also presynaptic to small-field medulla neurons in stratum M6, including Tm5 (Figures 7B and 7E–7H), and at a few contacts to a cell that resembles Tm9. In summary, the wide-field Dm8 neuron serves as a major target neuron for R7 input and provides output locally in stratum M6 to small-field projection neurons.

DISCUSSION

Anatomical and Functional Mapping of Chromatic Visual Circuits

Previous studies using serial-section EM determined the detailed synaptic connections between R1–R6 photoreceptors and their target neurons in the lamina neuropil (Meinertzhagen and O'Neil, 1991; Meinertzhagen and Sorra, 2001). Based on this circuit information, a recent functional study provided considerable insight into the neural mechanisms of motion detection (Rister et al., 2007). In contrast, little was known about the synaptic target neurons of the R7 and R8 photoreceptors and the chromatic pathways their connection patterns subserved. This deficit reflected our inability until recently to penetrate the medulla's complexity (Fischbach and Dittrich, 1989). In this study, we made use of prior knowledge of neurotransmitters and their receptors in the visual system to design corresponding promoter constructs that identify the first-order interneurons. We then labeled these neurons with genetically encoded markers and analyzed their morphology and synaptic connections at the light and electron microscopic levels. Finally, we combined promoter dissection and the Split-Gal4 system with neurotransmitter hemidriviers to target particular neuron subtypes. We envision that the same combinatorial approach can be applied to dissect other complex neural circuits.

Projection Neurons Integrate Chromatic and Achromatic Channel Inputs and Relay Information to the Higher Visual Centers

In this study, we identified four types of transmedulla neurons, Tm5a/b/c, Tm9, Tm20, and Tm2, which express *Ort* and are therefore qualified to receive direct input from R7 or R8. These Tm neurons arborize in the medulla and project axons to the lobula, suggesting that they relay spectral information from the medulla to the lobula. Supporting this interpretation, we found that HA-syt, a presynaptic marker, is indeed localized to their terminals in the lobula. These data support previous suggestions that the lobula plays a key role in processing chromatic information for color vision (Bausenwein et al., 1992). Lobula stratum

5 appears most critical for color vision because it receives all three subtypes of Tm5 neurons, as well as Tm20. Moreover, we observed that HA-syt also localized to the dendrite-like processes of all Tm neurons in the proximal medulla, suggesting the presence of presynaptic sites at this level, too. Especially, Tm5a, Tm5b, and Tm20 all extend processes with this presynaptic marker in medulla stratum M8, supporting a previous notion that this stratum might receive chromatic information (Bausenwein et al., 1992).

All three subtypes of Tm5 neurons extend processes in medulla strata M6 and M3, suggesting that, there, they might be postsynaptic to R7 and R8 or L3. Using serial EM, we partially reconstructed a Tm5 subtype that receives direct synaptic input from both the chromatic UV channel of R7 and the achromatic channel of L3. Serial EM also revealed that Tm9 receives inputs from the chromatic green/blue channel of R8, as well as the achromatic L3 channel. It is tempting to speculate that the Tm9 and Tm5 neurons function as color-opponent neurons by subtracting the L3-mediated luminance signal from the R7/R8 chromatic signal (Figure 8). While the detailed neural mechanism must await electrophysiological studies, these anatomical data provide direct evidence that the achromatic and chromatic channels are not segregated, as previously proposed (Strausfeld and Lee, 1991). Instead, they converge on the first-/second-order interneurons early in the visual pathway.

The Amacrine Neuron Dm8 Is Required for UV Preference

Using a quantitative spectral preference test, we determined that, in flies, the Dm8 neurons are both necessary and sufficient to confer the animal's UV preference. Each Dm8 receives direct synaptic input from ~14 UV-sensing R7s. By pooling multiple R7 inputs, the Dm8 neurons may achieve high UV sensitivity at the cost of spatial resolution. Consistent with this notion, Dm8 is a main postsynaptic partner for R7 terminals; essentially all of R7's presynaptic sites contain at least one Dm8 postsynaptic element. The processes of Dm8 and their synapses with R7s are largely restricted to the medulla stratum M6. The stratum-specific arborization of Dm8 readily explains why R7 photoreceptors that fail to project axons to the M6 stratum are incapable of conferring UV preference (Lee et al., 2001; Clandinin et al., 2001).

Dm8 itself has no direct output to higher visual centers in the lobula; instead, it is presynaptic to small-field projection neurons, such as Tm5 and possibly Tm9, in the medulla (Figure 8). Thus, Dm8 provides lateral connections linking projection neurons. The morphologies and connections of Dm8 are thus reminiscent of those made by horizontal and amacrine cells in the vertebrate retina (Dowling, 1987). The vertebrate horizontal cells form reciprocal synapses with multiple cones, and, in the case where the cones are of different spectral types, the horizontal cells can establish color opponency, as demonstrated in the goldfish retina (Stell et al., 1975). Dm8 in *Drosophila* receives inputs from both Rh3- and Rh4-expressing R7s but does not provide feedback to photoreceptor terminals, suggesting that Dm8 is unlikely to contribute to color opponency, at least not in a way analogous to vertebrate horizontal cells. Vertebrate amacrine cells have diverse subtypes, which carry out very

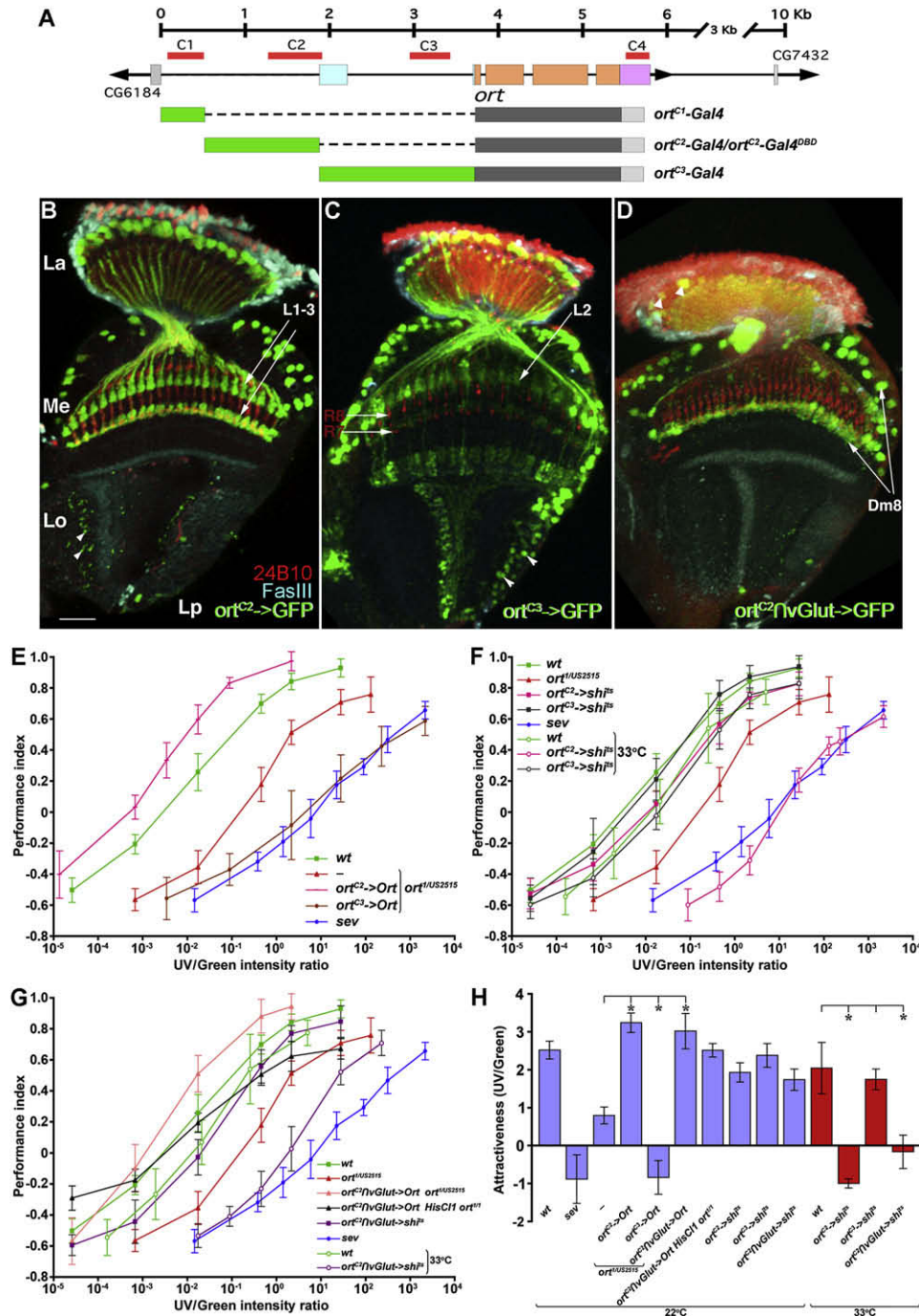


Figure 6. Wide-Field Dm8 Amacrine Neurons Are Required for UV Preference

(A) Various *ort* promoter constructs containing different multispecies-conserved regions (C1–C3). The *ort* locus structure is as described in Figure 1E. (B–D) Expression patterns of *ort*^{C2}-GAL4 (B), *ort*^{C3}-GAL4 (C), and *ort*^{C2}∩*vGlut* (D) drivers in adult optic lobes. These drivers were used to express the mCD8-GFP marker in different subsets of Ort-expressing neurons (see text for details). A few neurons in the lobula and lobula plate (arrowheads), which do not normally express Ort, were labeled by *ort*^{C2}-GAL4 and *ort*^{C3}-GAL4, respectively (B and C). (D) The combinatorial driver *ort*^{C2}∩*vGlut* labeled Dm8, as well as sparse L1 cells (arrowheads in lamina cortex). (Red) Photoreceptor axons visualized with MAB24B10 antibody. (Cyan) Specific medulla and lobula strata immunolabeled with anti-FasIII. Scale bar, 20 μm in (B) for (B–D). (E–H) Restoring or blocking different subsets of Ort-expressing neurons affects UV/green preference. Intensity-response curves were measured as described in Figure 2. (E–G) Error bars (standard deviations) represent the variations among trials. (E) Sufficiency of *ort*^{C2} and *ort*^{C3} neurons for UV/green preference. Restoring the function to the *ort*^{C2} neuron subset rescued UV preference in *ort* mutants, while restoring it to the *ort*^{C3} subset rendered a stronger green preference. *ort*^{1/US2515}, wild-type, and negative control *sev* data are from Figure 2E.

different functions, including correlating firing among ganglion cells, modulating center-surround balance of the ganglion cells, and direction selectivity (MacNeil and Masland, 1998; Meister et al., 1995; Yoshida et al., 2001; Nirenberg and Meister, 1997; He and Masland, 1997). The amacrine cells in vertebrate retina receive inputs from bipolar cells and provide the main synaptic input to ganglion cells. Thus, it is interesting to note that, while direct synaptic connections from R7s to Tm5 projection neurons exist, the indirect information flow from R7 to Dm8 and then to Tm5 is both necessary and sufficient to confer UV preference, as suggested by our inactivating and restoring experiments (Figure 8). We hypothesize that the direct and indirect pathways function at different UV intensity levels; Dm8 pools multiple R7 inputs to detect low-intensity UV in the presence of high-intensity visible light, while, under high-intensity UV, Tm5 receives direct input from R7 and mediates true color vision. Further studies using electrophysiology or functional imaging would be required to determine the neural mechanisms of Dm8.

The spectral preference assay used in this study and others measures relative “attractiveness” of UV and green light and, therefore, depends on the visual subsystems sensing UV and green light, as well as the interactions between these subsystems (Schümperli, 1973; Fischbach, 1979). While in simple phototaxis assays, the broad-spectrum and most-sensitive photoreceptors, R1–R6, dominate simple phototactic response to both UV and green light, they, as well as their first-order interneurons L1 and L2, appear to play an insignificant or redundant role in spectral preference. Thus, R8 alone, or together with R1–R6, provides the sensory input to promote green phototaxis and/or antagonize UV attraction. The first-order interneurons that relay R8 input in this context have yet to be identified. While our anatomical analysis revealed that Tm9 receives direct synaptic input from R8, the behavioral studies provided only weak and circumstantial evidence for its role in spectral preference.

Expressing *Ort* using the *chaOrt^{C1-3}* or *ort^{C3}-Gal4* driver significantly reduced UV preference in *ort* mutants, and Tm9 is covered by both drivers. Furthermore, inactivating Tm9 using the *ort^{C3}* driver and *sh^{ts1}* did not affect UV preference, suggesting that other neurons, such as Tm20, might function redundantly. Verification of these suggestions must await the isolation of Tm9- and Tm20-specific drivers and the corresponding behavioral studies to assay the effects of perturbing activity in these neurons. It is worth noting that *Ort*-expressing neurons do not include any Dm8-like wide-field neurons for R8s, and restoring activity in the *ort^{C3}* neuron subset is sufficient to confer stronger green preference in *ort* mutants. Thus, it is tempting to speculate that Dm8 circuits evolved uniquely to meet the ecological need to detect dim UV against a background of ample visible light.

EXPERIMENTAL PROCEDURES

Comparative Genomic Analyses

Comparative genomic analyses were carried out as previously reported (Odenwald et al., 2005; Yavatkar et al., 2008). See Supplementary Experimental Procedures for details.

Generation of *Ort* and *HisCl1* Promoter Constructs and Transgenic Flies

Ort and *HisCl1* promoter fragments were PCR amplified from genomic DNA of wild-type Oregon-R flies and were used to generate various *ort* promoter-*Gal4*, *LexA::VP16*, and *HisCl1-Gal4* constructs (Figures 1, 6, and S3). Cloning procedures are described in the Supplementary Experimental Procedures. Transgenic flies were generated using standard injection procedures by Rainbow Transgenic Flies, Inc. (Newbury Park, CA).

Fly Stocks

The genotypes of fly lines and rearing conditions are described in Supplementary Experimental Procedures.

Generation of Single-Neuron Clones

To label single neurons, we used the *hs-Flp* and *UAS > CD2,y+ > mCD8-GFP* transgenes (Wong et al., 2002) in combination with various *ort* promoter-*Gal4* or split-*Gal4* drivers. To assess in single neurons the distribution of the presynaptic marker, HA-tagged synaptotagmin (a generous gift from Drs. Christopher Potter and Liqun Luo), we used a similar flip-out strategy to that described above but implemented the strategy using *Tub > Gal80 >*. Flies carrying the transgenes *hs-Flp*, *UAS-Syt-HA*, *UAS-mCD8GFP*, *Tub > Gal80 >*, and *ort^{C1-3}-Gal4* (or *ort^{C2}-Gal4*) were used. Larvae of suitable genotypes at the late second- or early third-instar stage were briefly heat-shocked at 38°C for 3 min to remove the flip-out cassette (*> CD2, y+ >*, or *> Gal80 >*) in a small number of neurons.

Confocal Imaging of Whole-Mount Brains

Confocal imaging was performed as described previously (Ting et al., 2005). See Supplementary Experimental Procedures for details.

Electron Microscopy

UAS-HRP-CD2 (a generous gift from Dr. Liqun Luo) was used to visualize *Gal4*-driven expression in identified neurons that was targeted to the plasmalemma (Larsen et al., 2003). To reveal HRP activity at the EM level, we used the DAB method and, after dissecting brains from the head capsule, exposed them to DAB, as previously reported (Clements et al., 2008). Serial-section EM of the medulla was then undertaken, also as previously reported (Takemura et al., 2008). Cells that expressed HRP had an electron-dense reaction product at their membranes. 3D EM reconstructions of Tm5, Tm2, Tm9, and Dm8 profiles were carried out based on an unlabeled series of 672 60 nm sections, which included the outer six strata of the medulla, as described previously (Takemura et al., 2008).

UV/Green Spectral Preference and Phototaxis Assays

The forced two-choice assay for testing a fly's phototaxis preference to UV or green light has been described previously (Ting et al., 2007). Fast phototaxis assay was performed as for the spectral preference assay except that only one light source was used. Detailed procedures are given in Supplementary Experimental Procedures.

(F) Requirement for *ort^{C2}* and *ort^{C3}* neurons for UV/green preference. Blocking the *ort^{C2}*, but not *ort^{C3}*, neuron subset in wild-type background reduced UV preference. *ort^{1/US2515}*, wild-type, and negative control *sev* data are from Figure 2E.

(G) Requirement for and sufficiency of the Dm8 neurons for UV/green preference. Restoring *Ort* expression in the Dm8 neurons using the *ort^{C2}∩vGlut* driver rescued UV preference defects in *ort* or *HisCl1 ort* double-null mutants. Conversely, inactivating the Dm8 neurons caused a significant reduction in UV preference. *ort^{1/US2515}*, wild-type, and negative control *sev* data are from Figure 2E.

(H) Histogram of the relative attractiveness of UV over green light ($\text{Attr}_{\text{UV/G}}$) calculated from (E–G). The differences between *ort* mutants and after *ort* function is rescued in *ort^{C2}- > Ort* (or *ort^{C3}- > Ort* or *ort^{C2}∩vGlut- > Ort*) are statistically significant ($p < 0.00001$), as are those between the wild-type and *ort^{C2}- > sh^{ts1}* (or *ort^{C2}∩vGlut- > sh^{ts1}*). Error bars indicate SD.

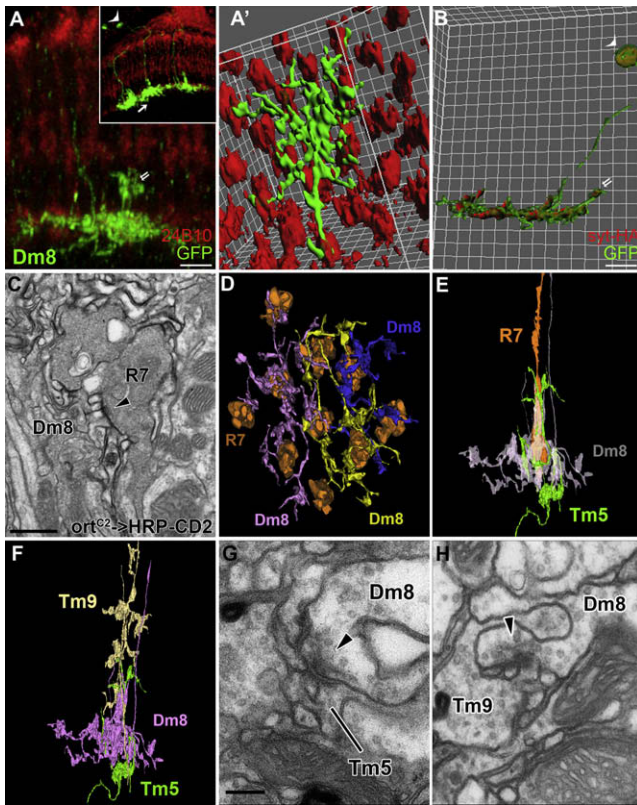


Figure 7. Amacrine Dm8 Neurons Receive Direct Synaptic Input from Multiple R7 Neurons

(A–A') Single Dm8 neuron clones were generated using *ort^{cs2}-Gal4, hs-Flp*, and *UAS- > CD2 > mCD8GFP* and visualized with anti-GFP antibody (green). Photoreceptor axons were visualized with MAb24B10 antibody (red). Dm8 neurons extend large processes in medulla stratum M6 (arrow, inset) where they are postsynaptic to 13–16 R7s (A') and presynaptic to Tm5s. In addition, each Dm8 extends small centrifugal processes to stratum M4, where they are presynaptic to Tm9 (double arrows, [A] and [B]). Demonstration of synaptic relations is shown from EM in later panels. (Inset) A low-magnification view of (A). The arrowhead and arrow indicate the Dm8 neuron shown in (A). (A') Isosurface representation of processes of a single Dm8 neuron in a proximodistal view. (B) Distribution of presynaptic sites of a single Dm8 neuron. Presynaptic reporter synaptotagmin-HA (red) was localized to the Dm8 processes in strata M6 and M4 (double arrows). (C) Dm8 is postsynaptic to R7s. A single EM section from stratum M6 shows Dm8 processes marked by an EM marker HRP-CD2 and stained with DAB. R7 terminal was identified based on its vesicle-laden ultrastructure, the presence of capitate projections (data not shown), and its location in stratum M6. Presynaptic T-bar ribbon (arrowhead) in R7 profile is juxtaposed to postsynaptic elements of Dm8 with electron-dense membranes. (D) Serial EM reconstruction of processes of three Dm8 neurons (pink, yellow, and blue) and corresponding R7 terminals (orange). The processes of Dm8 neurons tile stratum M6 with partial overlapping so that each R7 is presynaptic to one or two Dm8 cells. (E and F) Profiles of R7 (orange), Dm8 (pink), Tm5 (green), and Tm9 (beige) reconstructed from a single medulla column. (G and H) Single EM sections show that Dm8 is presynaptic to Tm5 (G) and Tm9 (H). Presynaptic T-bar ribbons in Dm8, indicated by arrowheads, point in the presumed direction of transmission. Scale bars: (A and B) 5 μ m; (C) 500 nm; 200 nm in (G) for (G) and (H).

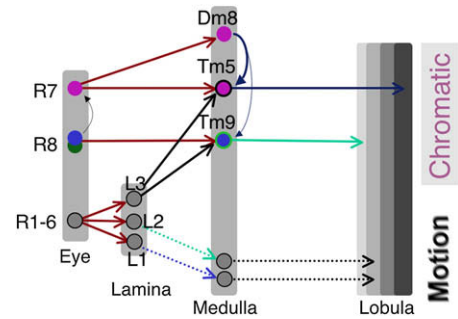


Figure 8. Medulla Circuits in Chromatic Information Processing

Summary diagram of synaptic connections between photoreceptor neurons and their first-order interneurons. Small-field projection neurons, Tm5 and Tm9, receive inputs from the chromatic channels, R7 and R8, respectively, as well as from the achromatic channel L3. Wide-field amacrine neuron Dm8 receives input from multiple R7s and is presynaptic to Tm5 and Tm9. In addition, R7 receives direct input from R8.

Head Yaw Optomotor Response Assay

The head yaw optomotor assay has been described (Rister et al., 2007). The modifications are described in Supplementary Experimental Procedures.

Electrophysiological Recording

Electroretinogram (ERG) recordings were taken using an electrophysiology set-up provided by Dr. Howard Nash (NIH), as described previously (Rajaram et al., 2005).

SUPPLEMENTAL DATA

The Supplemental Data include Supplemental Experimental Procedures and seven figures and can be found with this article online at [http://www.neuron.org/supplemental/S0896-6273\(08\)00705-8](http://www.neuron.org/supplemental/S0896-6273(08)00705-8).

ACKNOWLEDGMENTS

We thank Drs. William Pak, Liquin Luo, Christopher Potter, Martin Heisenberg, Tzumin Lee, Robert White, Akinao Nose, Howard Nash, Jaeseob Kim, Gero Miesenböck, and Alan Wong for reagents. We thank Drs. Claude Desplan and Javier Morante for communicating results prior to publication. We thank Dr. Howard Nash and Robert Scott for helping with ERG recordings and for providing the optomotor equipment. We thank Tom Pohida and Randall Pursley for optimizing the pattern recognition software and Jimmie Powell and Howard Metger for instrument fabrication. We thank Mr. Louis Dye and Dr. James Russell at NICHD's Microscopy and Image Core for assistance with EM image collection. We thank Drs. Alan Hinnebusch, Mark Stopfer, and Henry Levin for helpful discussion and Margaret Dieringer and Laura Lee for editing and manuscript handling. This work was supported by the Intramural Research Program of the NIH, National Institute of Child Health and Human Development (grant HD008748-03 to C.-H.L.), by the German Science Foundation (GRK 1156 and SFB 554 to J.R.), and by a grant from the National Eye Institute of the NIH (EY-03592 to I.A.M.).

Accepted: August 15, 2008
Published: October 22, 2008

REFERENCES

Bausenwein, B., Dittrich, A.P., and Fischbach, K.F. (1992). The optic lobe of *Drosophila melanogaster*. II. Pathways in the medulla. *Cell Tissue Res.* 267, 17–28.

- Campos-Ortega, J.A., and Strausfeld, N.J. (1972). The columnar organization of the second synaptic region of the visual system of *Musca domestica*. L.I. Receptor terminals in the medulla. *Z. Zellforsch. Mikrosk. Anat.* **124**, 561–585.
- Clandinin, T.R., Lee, C.-H., Herman, T., Lee, R.C., Yang, A.Y., Ovasapyan, S., and Zipursky, S.L. (2001). *Drosophila* LAR regulates R1–R6 and R7 target specificity in the visual system. *Neuron* **32**, 237–248.
- Clements, J., Lu, Z., Gehring, W.J., Meinertzhagen, I.A., and Callaerts, P. (2008). Central projections of photoreceptor axons originating from ectopic eyes in *Drosophila*. *Proc. Natl. Acad. Sci. USA* **105**, 8968–8973.
- Coombe, P.E., and Heisenberg, M. (1986). The structural brain mutant *Vacuolar medulla* of *Drosophila melanogaster* with specific behavioral defects and cell degeneration in the adult. *J. Neurogenet.* **3**, 135–158.
- Dowling, J.E. (1987). *The Retina* (Cambridge: Harvard University Press).
- Fischbach, K.F. (1979). Simultaneous and successive colour contrast expressed in “slow” phototactic behaviour of walking *Drosophila melanogaster*. *J. Comp. Physiol.* **130**, 161–171.
- Fischbach, K.F., and Dittrich, A.P. (1989). The optic lobe of *Drosophila melanogaster*. I. A Golgi analysis of wild-type structure. *Cell Tissue Res.* **258**, 441–475.
- Gengs, C., Leung, H.T., Skingsley, D.R., Iovchev, M.I., Yin, Z., Semenov, E.P., Burg, M.G., Hardie, R.C., and Pak, W.L. (2002). The target of *Drosophila* photoreceptor synaptic transmission is a histamine-gated chloride channel encoded by *ort* (*hclA*). *J. Biol. Chem.* **277**, 42113–42120.
- Gisselmann, G., Pusch, H., Hovemann, B.T., and Hatt, H. (2002). Two cDNAs coding for histamine-gated ion channels in *D. melanogaster*. *Nat. Neurosci.* **5**, 11–12.
- Goldsmith, T.H. (1961). *The Color Vision of Insects* (Baltimore: The Johns Hopkins University Press).
- Hardie, R.C. (1979). Electrophysiological analysis of fly retina. I: Comparative properties of R1–6 and R7 and R8. *J. Comp. Physiol.* **129**, 19–33.
- Hardie, R.C. (1987). Is histamine a neurotransmitter in insect photoreceptors? *J. Comp. Physiol. [A]* **161**, 201–213.
- He, S., and Masland, R.H. (1997). Retinal direction selectivity after targeted laser ablation of starburst amacrine cells. *Nature* **389**, 378–382.
- Heisenberg, M., and Buchner, E. (1977). The role of retinula cell types in visual behavior of *Drosophila melanogaster*. *J. Comp. Physiol.* **117**, 127–162.
- Hu, K.G., and Stark, W.S. (1977). Specific receptor input into spectral preference in *Drosophila*. *J. Comp. Physiol.* **121**, 241–252.
- Jacob, K.G., Willmund, R., Folkers, E., Fischbach, K.F., and Spatz, H.Ch. (1977). T-maze phototaxis of *Drosophila melanogaster* and several mutants in the visual systems. *J. Comp. Physiol.* **116**, 209–225.
- Kitamoto, T. (2001). Conditional modification of behavior in *Drosophila* by targeted expression of a temperature-sensitive *shibire* allele in defined neurons. *J. Neurobiol.* **47**, 81–92.
- Larsen, C.W., Hirst, E., Alexandre, C., and Vincent, J.P. (2003). Segment boundary formation in *Drosophila* embryos. *Development* **130**, 5625–5635.
- Lee, C.H., Herman, T., Clandinin, T.R., Lee, R., and Zipursky, S.L. (2001). N-cadherin regulates target specificity in the *Drosophila* visual system. *Neuron* **30**, 437–450.
- Luan, H., Peabody, N.C., Vinson, C.R., and White, B.H. (2006). Refined spatial manipulation of neuronal function by combinatorial restriction of transgene expression. *Neuron* **52**, 425–436.
- Luo, L., Callaway, E.M., and Svoboda, K. (2008). Genetic dissection of neural circuits. *Neuron* **57**, 634–660.
- MacNeil, M.A., and Masland, R.H. (1998). Extreme diversity among amacrine cells: implications for function. *Neuron* **20**, 971–982.
- Meinertzhagen, I.A. (1976). The organization of perpendicular fibre pathways in the insect optic lobe. *Philos. Trans. R. Soc. Lond. B Biol. Sci.* **274**, 555–594.
- Meinertzhagen, I.A., and O’Neil, S.D. (1991). Synaptic organization of columnar elements in the lamina of the wild type in *Drosophila melanogaster*. *J. Comp. Neurol.* **305**, 232–263.
- Meinertzhagen, I.A., and Sorra, K.E. (2001). Synaptic organisation in the fly’s optic lamina: few cells, many synapses and divergent microcircuits. *Prog. Brain Res.* **131**, 53–69.
- Meister, M., Lagnado, L., and Baylor, D.A. (1995). Concerted signaling by retinal ganglion cells. *Science* **270**, 1207–1210.
- Menzel, R. (1979). Spectral sensitivity and colour vision in invertebrates. In *Vision in Invertebrates* (Handbook of Sensory Physiology, Volume VII/6A), H. Autrum, ed. (New York: Springer Verlag), pp. 503–580.
- Menzel, R., and Greggers, U. (1985). Natural phototaxis and its relationship to colour vision in honeybees. *J. Comp. Physiol.* **157**, 311–321.
- Menzel, R., and Backhaus, W. (1991). Colour vision in insects. In *Vision and Visual Dysfunction. The Perception of Colour*, P. Gouras, ed. (London: MacMillan), pp. 262–288.
- Mikeladze-Dvali, T., Desplan, C., and Pistillo, D. (2005). Flipping coins in the fly retina. *Curr. Top. Dev. Biol.* **69**, 1–15.
- Morante, J., and Desplan, C. (2008). The color-vision circuit in the medulla of *Drosophila*. *Curr. Biol.* **18**, 553–565.
- Nirenberg, S., and Meister, M. (1997). The light response of retinal ganglion cells is truncated by a displaced amacrine circuit. *Neuron* **18**, 637–650.
- Odenwald, W.F., Rasband, W., Kuzin, A., and Brody, T. (2005). EVOPRINTER, a multigenomic comparative tool for rapid identification of functionally important DNA. *Proc. Natl. Acad. Sci. USA* **102**, 14700–14705.
- Orger, M.B., and Baier, H. (2005). Channeling of red and green cone inputs to the zebrafish optomotor response. *Vis. Neurosci.* **22**, 275–281.
- O’Tousa, J.E., Baehr, W., Martin, R.L., Hirsh, J., Pak, W.L., and Applebury, M.L. (1985). The *Drosophila ninaE* gene encodes an opsin. *Cell* **40**, 839–850.
- Pantazis, A., Segaran, A., Liu, C.H., Nikolaev, A., Rister, J., Thum, A.S., Roeder, T., Semenov, E., Juusola, M., and Hardie, R.C. (2008). Distinct roles for two histamine receptors (*hclA* and *hclB*) at the *Drosophila* photoreceptor synapse. *J. Neurosci.* **28**, 7250–7259.
- Pollack, I., and Hofbauer, A. (1991). Histamine-like immunoreactivity in the visual system and brain of *Drosophila melanogaster*. *Cell Tissue Res.* **266**, 391–398.
- Rajaram, S., Scott, R.L., and Nash, H.A. (2005). Retrograde signaling from the brain to the retina modulates the termination of the light response in *Drosophila*. *Proc. Natl. Acad. Sci. USA* **102**, 17840–17845.
- Rister, J., Pauls, D., Schnell, B., Ting, C.Y., Lee, C.H., Sinakevitch, I., Morante, J., Strausfeld, N.J., Ito, K., and Heisenberg, M. (2007). Dissection of the peripheral motion channel in the visual system of *Drosophila melanogaster*. *Neuron* **56**, 155–170.
- Salcedo, E., Huber, A., Henrich, S., Chadwell, L.V., Chou, W.H., Paulsen, R., and Britt, S.G. (1999). Blue- and green-absorbing visual pigments of *Drosophila*: ectopic expression and physiological characterization of the R8 photoreceptor cell-specific Rh5 and Rh6 rhodopsins. *J. Neurosci.* **19**, 10716–10726.
- Sarthy, P.V. (1991). Histamine: a neurotransmitter candidate for *Drosophila* photoreceptors. *J. Neurochem.* **57**, 1757–1768.
- Schümperli, R.A. (1973). Evidence for colour vision in *Drosophila melanogaster* through spontaneous phototactic choice behaviour. *J. Comp. Physiol.* **86**, 77–94.
- Shinza-Kameda, M., Takasu, E., Sakurai, K., Hayashi, S., and Nose, A. (2006). Regulation of layer-specific targeting by reciprocal expression of a cell adhesion molecule, capricious. *Neuron* **49**, 205–213.
- Stell, W.K., Lightfoot, D.O., Wheeler, T.G., and Leeper, H.F. (1975). Goldfish retina: functional polarization of cone horizontal cell dendrites and synapses. *Science* **190**, 989–990.
- Storz, U.C., and Paul, R.J. (1998). Phototaxis in water fleas (*Daphnia magna*) is differently influenced by visible and UV light. *J. Comp. Physiol. [A]* **183**, 709–717.
- Strausfeld, N.J., and Lee, J.K. (1991). Neuronal basis for parallel visual processing in the fly. *Vis. Neurosci.* **7**, 13–33.

- Takemura, S.Y., Lu, Z., and Meinertzhagen, I.A. (2008). Synaptic circuits of the *Drosophila* optic lobe: the input terminals to the medulla. *J. Comp. Neurol.* 509, 493–513.
- Ting, C.Y., Yonekura, S., Chung, P., Hsu, S.N., Robertson, H.M., Chiba, A., and Lee, C.H. (2005). *Drosophila* N-cadherin functions in the first stage of the two-stage layer-selection process of R7 photoreceptor afferents. *Development* 132, 953–963.
- Ting, C.Y., Herman, T., Yonekura, S., Gao, S., Wang, J., Serpe, M., O'Connor, M.B., Zipursky, S.L., and Lee, C.H. (2007). Tiling of R7 axons in the *Drosophila* visual system is mediated both by transduction of an activin signal to the nucleus and by mutual repulsion. *Neuron* 56, 793–806.
- Tomlinson, A., and Ready, D.F. (1986). Sevenless: A cell-specific homeotic mutation of the *Drosophila* eye. *Science* 231, 400–402.
- Witte, I., Kreienkamp, H.J., Gewecke, M., and Roeder, T. (2002). Putative histamine-gated chloride channel subunits of the insect visual system and thoracic ganglion. *J. Neurochem.* 83, 504–514.
- Wong, A.M., Wang, J.W., and Axel, R. (2002). Spatial representation of the glomerular map in the *Drosophila* protocerebrum. *Cell* 109, 229–241.
- Yamaguchi, S., Wolf, R., Desplan, C., and Heisenberg, M. (2008). Motion vision is independent of color in *Drosophila*. *Proc. Natl. Acad. Sci. USA* 105, 4910–4915.
- Yavatkar, A.S., Lin, Y., Ross, J., Fann, Y., Brody, T., and Odenwald, W.F. (2008). Rapid detection and curation of conserved DNA via enhanced-BLAT and EvoPrinterHD analysis. *BMC Genomics* 9, 106–118.
- Yoshida, K., Watanabe, D., Ishikane, H., Tachibana, M., Pastan, I., and Nakanishi, S. (2001). A key role of starburst amacrine cells in originating retinal directional selectivity and optokinetic eye movement. *Neuron* 30, 771–780.
- Zheng, Y., Hirschberg, B., Yuan, J., Wang, A.P., Hunt, D.C., Ludmerer, S.W., Schmatz, D.M., and Cully, D.F. (2002). Identification of two novel *Drosophila melanogaster* histamine-gated chloride channel subunits expressed in the eye. *J. Biol. Chem.* 277, 2000–2005.

Supplemental Data

The Neural Substrate of Spectral Preference in *Drosophila*

Shuying Gao, Shin-ya Takemura, Chun-Yuan Ting, Songling Huang, Zhiyuan Lu, Haojiang Luan, Jens Rister, Andreas S. Thum, Meiluen Yang, Sung-Tae Hong, Jing W. Wang, Ward F. Odenwald, Benjamin H. White, Ian A. Meinertzhagen, and Chi-Hon Lee

Supplemental Experimental Procedures

Comparative genomic analyses were carried out as previously reported (Odenwald et al., 2005; Yavatkar et al. 2008). Briefly, genomic regions (supplementary Figure 2) encompassing the *ort* and *HisCII* genes from 12 *Drosophila* species were aligned using enhanced-BLAT program and analyzed using the *EvoPrinterHD* algorithms (Yavatkar et al. 2008). *Drosophila melanogaster* nucleotide residues that are conserved in at least 11 *Drosophila* species were highlighted with bold uppercase letters (supplementary Figure 2). Conserved regions (C1-C4 in *ort* and C1-C2 in *HisCII* genes; underlined in supplementary Figure 2) were assigned by manually clustering the MCSs and excluding the coding regions.

Transgene constructions

Ort and *HisCII* promoter fragments were PCR amplified from genomic DNA of wild-type Oregon-R flies and were used to generate various *ort* promoter-Gal4, LexA::VP16 and *HisCII-Gal4* constructs (Figures 1, 6 and S3). Genomic sequences of *ort* and *HisCII* genes are shown in Figure S2. Nucleotide sequences were verified by sequencing. Detailed maps are available upon request.

Cloning procedures are described as follows:

(1) For *ort*^{C1-3}-*Gal4* and *ort*^{C1-3}-*LexA::VP16*, the following PCR primers were used to amplify the *ort* promoter and to introduce restriction sites (Asp718 at 5' and BamH I, Not I, Xho I at 3'; underlined):

Forward: 5'-GAGCGGGTACCGCCAAACACAAGTAAAAAGTTTGCT-3';

Reverse: 5'-GGATTCTCGAGGCGGCCGCGGATCCTTTAATGTGAGCTCTTTCTG
TGTGG-3'

The C1-3 fragment of the *ort* promoter was cloned into Asp718/Xho I sites of *pCaSpeR4* and the *Gal4* cDNA, isolated from pGaTB, was subsequently subcloned (via Bam HI and Not I site) into the resulting vector to generate *pCaSpeR4-ort*^{C1-3}-*Gal4*. The *LexA::VP16* cDNA was isolated from *pLot-LexA::VP16* (a generous gift from Tzumin Lee, UMass Medical School) and used to replace the *Gal4* cDNA in *pCaSpeR4-ort*^{C1-3}-*Gal4* (via Bam HI and Not I sites).

(2) For *ort*^{C1-4}-*Gal4*, the following primers were used to amplify the *ort* 3'UTR fragment, which contains the C4 conserved region, and to introduce Sal I and Not I restriction sites (underlined).

Forward: 5'-GTCGACTACGACGACTGTGCCCTGTA-3'.

Reverse: 5'-GCGGCCCGCCCAACCGGCTGAGAAATAGT -3'.

The *ort* 3'UTR fragment was used to replace the *hsp70* 3'UTR in the *pCaSpeR4-ort*^{C1-3}-*Gal4* (via Sal I/Not I sites), resulting in *pCaSpeR4-ort*^{C1-4}-*Gal4*.

(3) For *ort*^{C1}-*Gal4*, the following primers were used to amplify the promoter fragment containing the C1 conserved region (Figure 6 and supplementary Figure 2) and the promoter fragment was then subcloned into the Asp 718 and Bam HI sites of *pCaSpeR4-ort*^{C1-3}-*Gal4* to replace the *ort*^{C1-3} promoter fragment.

Forward: 5'-GAGCGGGTACCGCCAAACACAAGTAAAAAGTTTGCT-3'

Reverse: 5'-GGATTGGATCC(ATTTGAATTTAAAACGT)GCCCACTCGCCCAAGA-
3'

(4) *ort*^{C2}-*Gal4* has been described previously as *ort-Gal4* (Hong et al. 2006).

(5) The *ort*^{C3}-*Gal4* was constructed in a similar fashion as that for *ort*^{C1}-*Gal4* except that the following primers were used to amplify the C3 region of the *ort* promoter:

Forward: 5'-GAGCGGGTACCTTGGTGAACTGTTCGTTTCGT-3'

Reverse: 5'-GGATTCTCGAGGCGGCCGCGGATCCTTTAATGTGAGCTCTTTCTGTGTGG-3'

(6) For *ort*^{C1-3}-*Gal4DBD*, the *ort* promoter C1-3 fragments were isolated from pCaSper4-*ort*^{C1-3}-*Gal4* and subcloned into the EcoR I and Not I sites of *X11* (Luan et al., 2006). For *ort*^{C2}-*Gal4DBD*, the following primers were used to amplify the *ort* promoter fragment that contains the C2 conserved region (Figure 6A), and to introduce EcoR I and Not I restriction sites (underlined), and then subcloned into *X11* as described above.

Forward: 5'-GCGAATTCGTGGCAGGTCTCTGGGATTC -3'

Reverse: 5'-CCGCGGCCGCGACAGTTGGTGGCGAAC -3'

(7) For *ort*^{C1-3}-*Gal4AD*, the Gal4 activation domain (Gal4AD) was isolated from *CCAP-Gal4AD* (Luan et al., 2006) and subcloned into the Not I and Asc I sites of *ort*^{C1-3}-*Gal4DBD*, replacing the Gal4DBD fragment.

(8) *UAS-ort*, which contains the *ort* cDNA under the control of the *UAS* promoter, has been described previously (Rister et al., 2007).

(9) The Split-Gal4 enhancer trap plasmid *pP{y+, dVP16AD}* was constructed using a modified version of the VP16AD fragment from the original Split Gal4 system. The new fragment (dVP16AD), which is codon-optimized for expression in *Drosophila*, was used to replace Gal80 in the *pP{y+, Gal80}* (a generous gift from Drs. Christopher Potter and Liqun Luo, Stanford University). To hop *P{y+, dVP16AD}* into the *vGlut* locus, we injected the plasmid into the *yw, vGlut*^{OK371}-*Gal4* line (Mahr and Aberle, 2006) and screened for transgenic flies for yellow+. The transgenic flies were then crossed with *yw; UAS-EGFP; Elav-Gal4DBD* flies (Luan et al. 2006) and the progenies were screened for vGlut expression patterns. This method is similar to the “transposon swap” method described previously (Sepp and Auld, 1999) but uses direct injection to avoid making laborious genetic crosses.

Fly stocks

Fly stocks were reared in a standard medium supplemented with β -carotene (0.295g/L). All flies were raised at 25°C except those bearing *UAS-shi^{ts1}* and *Gal4* transgenes. The latter were reared at 18°C before experiments to avoid potential developmental defects. For behavioral experiments, flies were outcrossed for three generations to wild-type Canton-S (kindly provided by Dr. Howard Nash, NIH) to reduce potential effects from the genetic background.

The following driver lines were used for labeling neurons: (1) *w*; *ort^{C1-3}-LexA::VP16*; (2) *yw*; *vGlut-dVP16AD*, *ort^{C1-3}-Gal4DBD/CyO*; (3) *ort^{C1-3}-GAL4AD*; *cha-Gal4DBD*; (4) *w*; *ort^{C2}-Gal4/TM6B* (described as *ort-Gal4* in Hong et al. 2006); (5) *yw*; *ort^{C3}-Gal4*; (6) *yw*; *vGlut-dVP16AD/CyO*; *ort^{C2}-Gal4DBD/TM3*; (7) *w*; *HisC11-Gal4/CyO*; *HisC11-Gal4/TM6B*; (8) *w*; *vGlut-Gal4* (described as OK371-Gal4 in Mahr and Aberle, 2006) ; (9) *w*; *cha-Gal4* (Yasuyama et al., 1995); (10) *w*; *GAD1-Gal4* (a generous gift from Dr. Gero Miesenbock, Yale University; Ng et al. 2002); (11) *TH-Gal4*; and (12) *Ddc-Gal4* (Friggi-Grelin et al. 2003).

The following marker lines were used in combination with the driver lines described above to label neurons (1) *w*; *LexAop-rCD2::GFP* (a generous gift from Dr. Tzumin Lee); (2) *yw*; *UAS-EGFP*; *UAS-mCD8GFP*; (3) *w*; *UAS-GFP^{nl}*; and (4) *yw*; *UAS-mCD8GFP*.

To block the function of specific neuron subsets and assay the behavioral consequences, the *UAS-shi^{ts1}* lines (Kitamoto, 2001) were used in combination with the following driver lines: (1) ; *ort^{C1-4}-Gal4*; (2) ; *vGlut-dVP16AD*, *ort^{C1-3}-Gal4DBD/CyO*; (3) *ort^{C1-3}-GAL4AD*; *cha-Gal4DBD*; (4) *w*; *Bl/CyO*; *ort^{C2}-Gal4/TM6B*; (5) ; *ort^{C3}-Gal4*; (6) *yw*; *vGlut-dVP16AD/CyO*; *ort^{C2}-Gal4DBD/TM3*; (7) *w*; *LIL2-A-Gal4* (Rister et al., 2007); (8) *w*; *Lot-shi^{ts1}*; *ort^{C1-3}-LexA::VP16*; (9) *Rh4-Gal4*; *Rh3-Gal4/CyO* (kindly provided by Dr. Claude Desplan, New York University).

For behavioral assays, the *Canton-S* strain was used as the wild-type control (kindly provided by Dr. Howard Nash, NIH). *sev^{E2}* and *Norpa³⁶* mutants (Bloomington Stock Center, Indiana) were used as negative controls. *HisC11¹³⁴* mutants and double mutants *HisC11¹³⁴ ort¹* have been described previously (Hong et al. 2006). *ort^{US2515}* and *ort^{P306}*, which are strong hypomorphic alleles, were kindly provided by Dr. William Pak, Purdue

University). *ort¹*, which is null, was obtained from the Bloomington Stock Center (Gengs et al., 2002). These mutants were out-crossed to *Canton-S* and the presence of mutations was confirmed by PCR analyses.

To restore the function of neuron subsets and assay the behavioral consequences, the following stocks were used: (1) ; *UAS-ort/CyO; ort^{US2515}*; (2) *w; ort^{C1-4}-Gal4/CyO; ort¹/TM3*; (3) *yw; vGlut-dVP16AD, ort^{C1-3}-Gal4DBD/CyO; ort¹/TM3*; (4) *ort^{C1-3}-GAL4AD;; cha-Gal4DBD, ort¹/TM3*; (5) *w;; ort^{C2}-Gal4, ort¹/TM3*; (6) *yw; ort^{C3}-Gal4; ort¹/TM3*; (7) *yw; vGlut-dVP16AD; ort^{C2}-Gal4DBD, ort¹/TM3*; and (8) *L1L2-A-Gal4; ort¹/TM3*.

Confocal imaging of whole-mount brains

Whole-mount dissection, immunohistochemistry, confocal imaging (using a Zeiss LSM510 META and Plan Neofluar objective 40x/1.3), image deconvolution (Huygens Professional, Scientific Volume Imaging, Hilversum, Netherlands) and 3D image rendering (Imaris, Bitplane, Zurich, Switzerland) were all performed as described previously (Ting et al., 2005). The following dilutions of primary antibodies were used: mAb24B10, 1:100 (DSHB); mouse anti-FasIII 7G10, 1:25 (DSHB); mAbNC82, 1:25 (DSHB); mouse anti-Dlg 4F3, 1:50 (DSHB), mouse anti-Connectin C1.427, 1:50 (a generous gift from Dr. Robert White, Cambridge University); rabbit anti-Caps, 1:200 (a generous gift from Dr. Akinao Nose, Tokyo University); rabbit anti-GFP, 1:500 (Torrey Pines Biolabs, East Orange, NJ); rat anti-HA, 1:300 (Roche, Indianapolis, IN); and rat anti-mouse CD8a, 1:200 (Invitrogen, Carlsbad, CA). The secondary antibodies including goat anti-rabbit, rat or mouse IgG coupled to Alexa 488, Alexa 568, or Alexa 647 (Molecular Probes, Eugene, OR) were used at 1:200.

UV/Green Spectral Preference and Phototaxis Assays

The UV/Green spectral preference was carried out using a T-maze device made of transparent plexiglass (Lee et al., 2001). Two arms of the T-maze, fitted with transparent polystyrene vials (Fisher), were illuminated with either UV or green high-efficiency light-emitting diodes (LEDs 370 nm and 525 nm; Roithner Lasertechnik, Vienna, Austria) as described in Ting et al. 2007. Light intensity was calibrated at a distance of 13 cm to the light source (the distance from the center of the T-maze to the light source) using a Goldilux GRP-1 photometer. UV irradiance (in $\mu\text{W}/\text{cm}^2$) was measured using the GAP-1 probe. The illuminance of the green light (in Lx) was measured using the GLP-1 probe. The spectral composition, $S(\lambda)$, of the green light, determined by a spectroradiometer (Photo Research SpectraScan PR-670), was used to convert the illuminance reading to irradiance using the following formula: Irradiance = Illuminance $\times \int S(\lambda) d\lambda / (6.83 \times \int S(\lambda) V(\lambda) d\lambda)$; $V(\lambda)$ being the relative spectral sensitivity of the human eye.

Flies were pre-adapted to 50Lx ($14 \mu\text{W}/\text{cm}^2$) white light for at least one hour before testing. They were then knocked into a small compartment in the T-maze. After the adapting light was switched off and the test UV and green lights switched on, the flies now in an agitated state, were allowed to enter the vials illuminated by either test light. After each test, the flies in each vial were counted and the Performance Index (P.I.) calculated from the numbers choosing UV (N_{UV}) or green (N_G) light by the following formula: P.I. = $(N_{UV} - N_G) / (N_{UV} + N_G)$. The few flies remaining in the center compartment were discounted. For each genotype, 8 trials (~30 flies of 3-7 days old per trial) were carried out for each point of the intensity ratio. Intensity-response curves were measured over eight orders of magnitude of a UV/green intensity ratio (10^{-5} - 2×10^4). Green light intensity (in irradiance) was kept constant at $0.253 \mu\text{W}/\text{cm}^2$ except at the maximum ratio (2176.7) at which it was reduced to $0.0363 \mu\text{W}/\text{cm}^2$ to accommodate the intensity limit of the UV LED. The entire apparatus was housed in a temperature-controlled chamber. For tests using *shi^{ts1}*, the flies were pre-incubated for 5 min in the chamber at a non-permissive temperature (33°C) before behavioral assays were undertaken. The remaining experiments, including the *shi^{ts1}* controls, were carried out at a permissive temperature of 22°C.

Fast phototaxis towards UV or green light was measured using the same device as for the UV/green spectral preference assay except for the following modifications: (1) only one light source (UV or green) was switched on; (2) flies were adapted to either dark or 300 Lx ($83 \mu\text{W}/\text{cm}^2$) white light for 1 hr before testing.

Head Yaw Optomotor Response Assay

The head yaw optomotor assay has been described (Rister et al. 2007). To automate the measurement of head yaw, the following modifications were made. Images of fly heads were captured using an infrared camera (Sony) under infrared LED illumination and digitalized (at 30 frames/sec) using a frame-grabbing card from National Instruments (Austin, TX, USA). The images were processed in real-time or in batches using a pattern-matching program developed in house using the machine vision package from National Instruments. Head yaw angle was calculated by comparing the experimental images with a reference image taken before the experiments. For each genotype, ten flies 3-7 days of age were tested four times each.

Achromatic motion stimuli were provided by a high contrast pattern of four vertical black stripes (12°) in a white background, printed with an HP Color Laserjet printer. The drum housing the striped pattern was rotated at a speed of $36^\circ/\text{sec}$, first clockwise for 30 sec and then counterclockwise. Illumination was provided using a ring light. The light radiance of the black stripes and the white background were 0.003 and $0.03 \text{ W}/(\text{Sr}\cdot\text{m}^2)$, respectively.

Negative geotaxis assay

To identify potential motor defects, flies were tested for their ability to climb upward in the absence of visual cues. Briefly, flies (~20 per trial) were placed in a 30-cm long transparent plastic tube kept in an upright position. After being knocked to the bottom, flies were allowed to climb up the tube for 10 sec. Video images were recorded using an infrared camera (Sony) linked to a Windows-based PC and the position of each fly was tracked in real-time using a tracking program (Viewpoint). Flies were tested against a dark or a dim white light background (7 Lx, $1.9 \mu\text{W}/\text{cm}^2$) with infrared illumination (870 nm). The distance each fly climbed in 8 sec was plotted. Approximately 300-400 flies were tested for each genotype.

Supplemental Figures and Legends

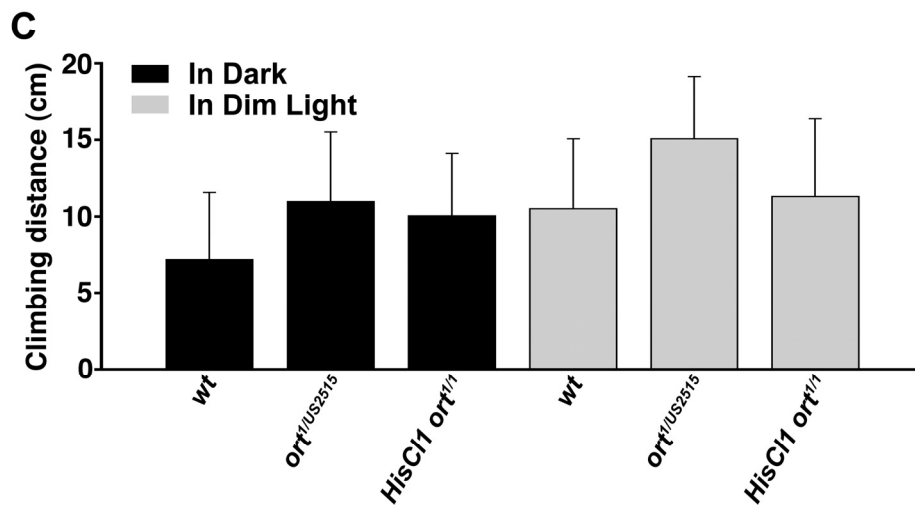
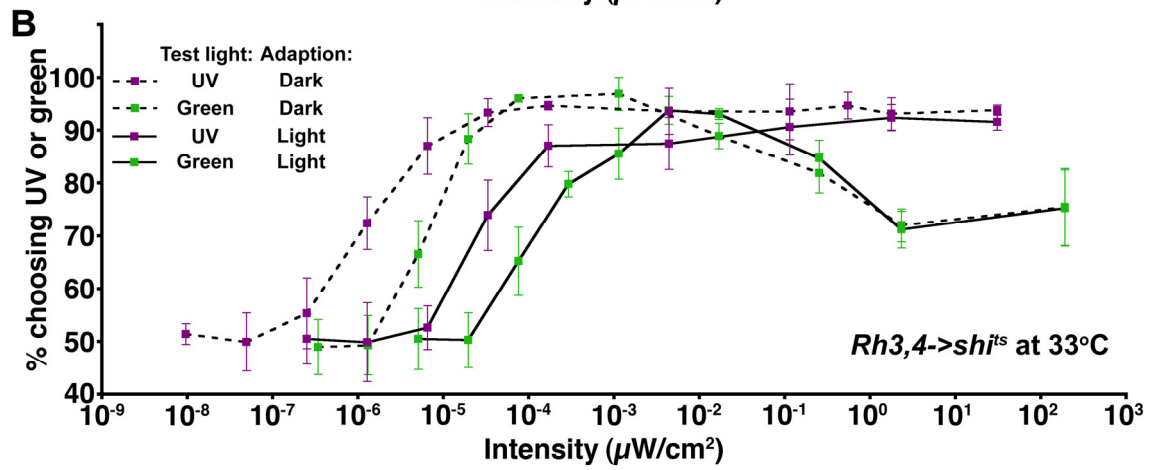
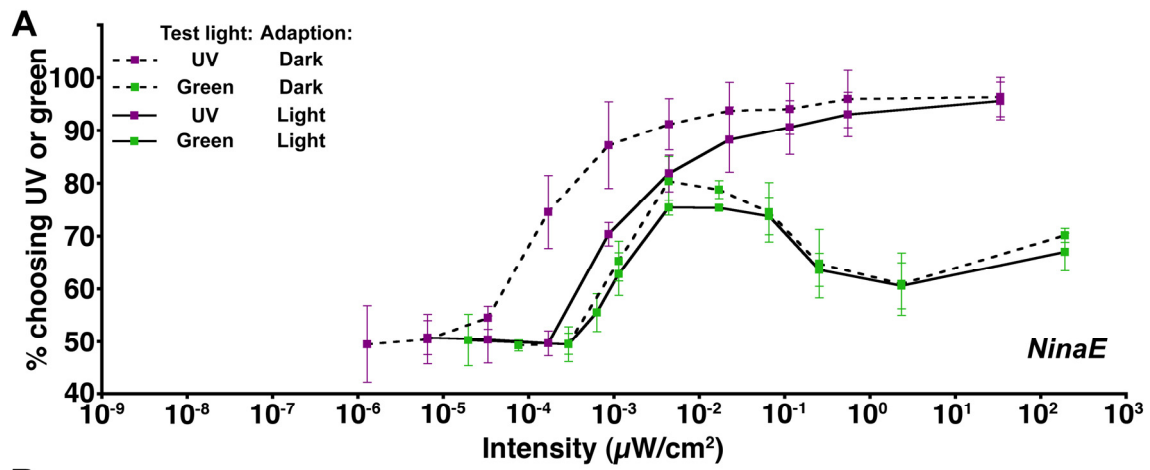


Figure S1. R1-R6 Photoreceptors Mediate Fast Phototaxis

(A-B) Mutants with defective R1-R6 or R7 functions were tested for fast phototaxis towards UV or green light as described in Figure 2A. The intensity-response curves were measured by recording the percentage of flies choosing UV or green light of various intensities over dark. Light intensity was shown as a logarithmic scale and error bars (standard deviations) represent the variations among trials.

(A) *NinaE* mutants, which lack the specific opsin for R1-R6, exhibited highly reduced phototactic responses to UV or green light. The intensity-response curves of *NinaE* mutants, when compared with those of wild-type (cf Figure 2A), were shifted to the right, and the maximal response towards green light failed to reach 100%.

(B) Inactivating R7s caused only a minor reduction in phototactic response towards UV. Flies carrying *Rh3,4->shi^{ts}* transgenes were tested for fast phototaxis at the non-permissive temperature. Their intensity-response curves resemble those of wild-type although the maximal response towards UV light was somewhat reduced under the light-adapted condition.

(C) *Ort* and *HisCII ort* double-null mutants exhibited no apparent motor defects. Motor functions of wild-type and *ort* and *HisCII¹³⁴ ort^l* double-null mutants were tested in negative geotaxis assays in darkness (black bars) or low light (grey bars) illumination. The average distance flies climbed in 8 sec was shown for each genotype. Error bars (standard deviation) represent variations among individual flies.

Figure S2. Comparative Genomic Sequence Analyses of the *ort* and *HisC11* Loci

EvoPrinterHD analyses of the *histamine chloride channel 2* (*ort*) (A), and *1* (*HisC11*) (B), loci of 12 *Drosophila* species (see Experimental Procedures for details). Only the genomic sequences from *Drosophila melanogaster* are shown. Highly conserved nucleotides (shared by at least 11 species) are identified with bold uppercase letters. The transcribed sequences are labeled as follows: 5'UTR (light blue), protein-encoding sequence (red), 3'UTR (dark blue) and introns (yellow).

(A) Outside the protein-encoding regions, the conserved sequences of the *ort* gene are clustered in four regions, C1-C4 (underlined). C1 and C2 are located in the intergenic region and C3 in the first intron. The *ort* promoter region containing C1-C3 gives rise to cell-specific expression patterns. C4, located in the 3'-UTR, contains several potential binding sites for micro-RNA, but does not appear to affect cell-type specific expression.

(B) Two conserved regions, C1 and C2, were identified in the first intron of the *HisC11* gene and the first intron of the neighboring gene, *CG17360*, respectively. The C2 region appears to be critical for driving glia-specific expression, which C1 alone fails to do (data not shown).

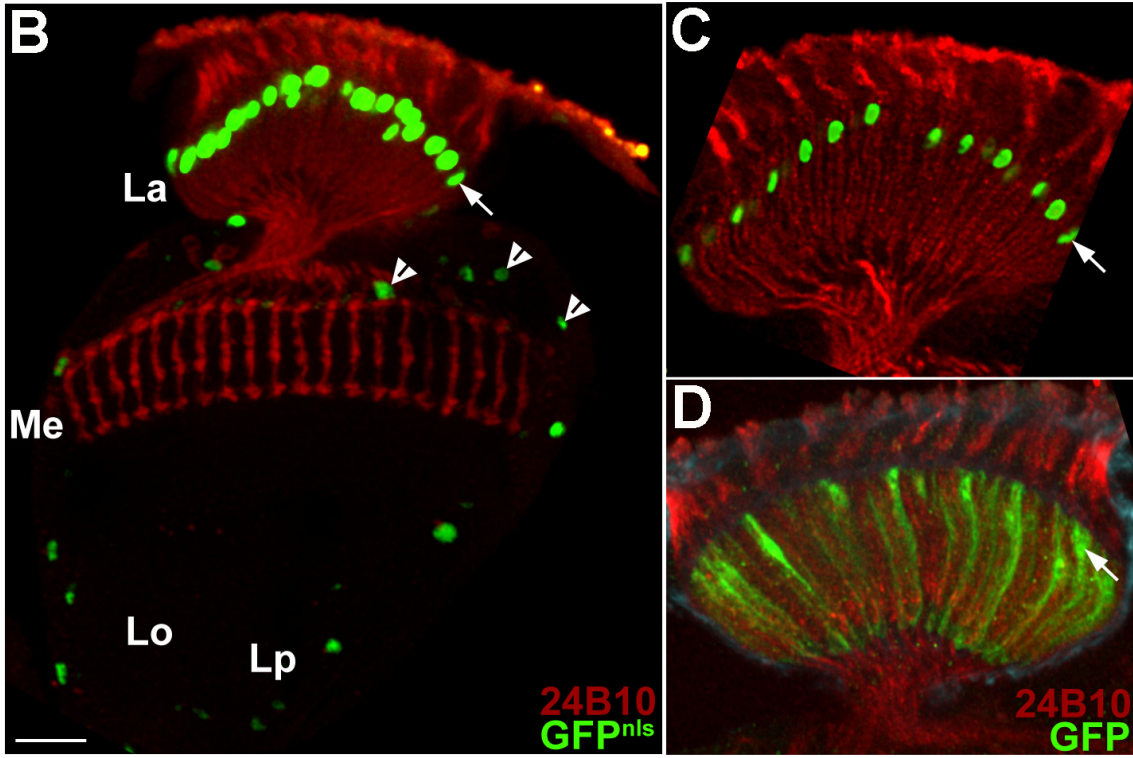
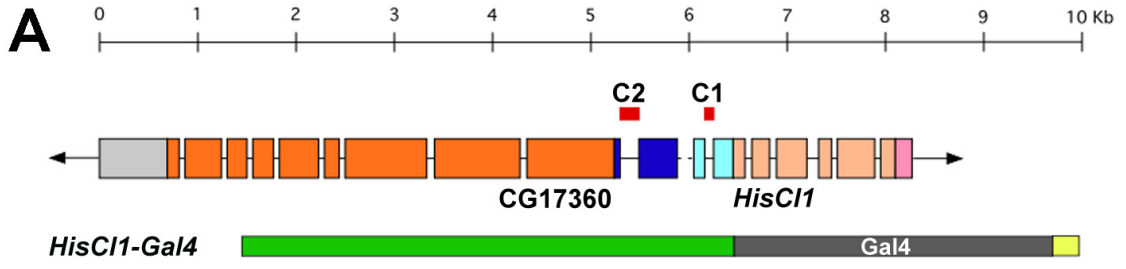


Figure S3. Histamine Chloride Channel 1 Is Expressed in Lamina Glia and Medulla Cells

(A) Promoter analysis of the *HisC11* gene. The *HisC11* genomic structure is shown as a linear cartoon: exons are indicated as boxes and introns and intergenic sequences as lines. Comparative genomic analysis identified two blocks of sequences (C1,C2; red boxes shown above the genomic structure) that are conserved in at least 11 out of 12 analyzed *Drosophila* species (see supplementary Figure 2). A large genomic region (green box) containing C1 and C2 as well as a part of the neighboring gene, *CG17360*, was fused to Gal4 (grey box) and *hs70* 3'UTR (yellow box) to generate the *HisC11-Gal4* driver.

(B-D) Expression pattern of *HisC11-Gal4* in the optic lobe. The *HisC11-Gal4* was used to drive the expression of nuclear-tagged GFP (GFP^{nl}s) (B,C) or cytoplasmic GFP (GFP) (D) markers (green). (C,D) High magnification views of the lamina. The *HisC11-Gal4* drives strong expression in lamina epithelial glia (arrows), with identifying nuclear locations in the distal lamina, which wrap around lamina cartridges (D). It is also expressed weakly in subsets of uncharacterized medulla cells (arrowheads) (B). Photoreceptors axons were visualized using MAb24B10 antibody (red).

Scale bar: in (B) 20 μ m.

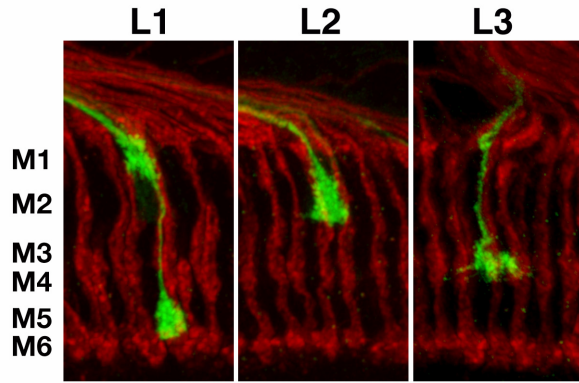
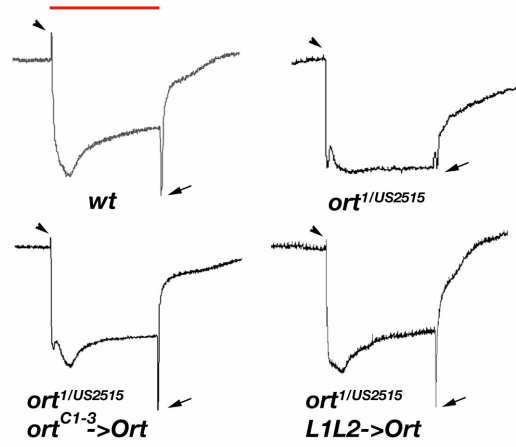
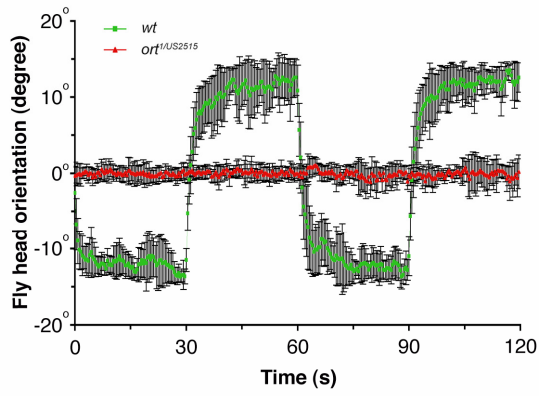
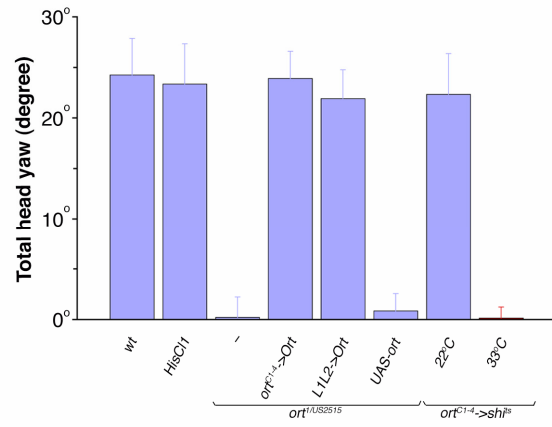
A**B****C****D**

Figure S4. The Histamine Chloride Channel Ort Is Expressed in the Lamina Neurons L1-L3 and Is Required for Motion Detection

(A) Axon terminals of L1, L2, and L3 mark different medulla strata. Single lamina L1-L3 neurons (green) were visualized using the *ort^{Cl-3}-Gal4* driver and the genetic mosaic system (*hs-Flp/UAS>CD2>mCD8-GFP*, see text for details). L1 terminals arborize in medulla strata M1 and M5, while L2 and L3 terminate in strata M2 and M3, respectively. Photoreceptor axons were visualized with MAb24B10 antibody (red) to mark the M3 and M6 strata.

(B) Expressing Ort using the *ort^{Cl-3}-Gal4* driver rescues electroretinogram (ERG) defects in *ort* mutants. The ‘on’- (arrowheads) and ‘off’-transients (arrows), which largely reflect the responses of lamina cells, were absent in *ort* mutants. Expressing Ort using the *ort^{Cl-3}-Gal4* or *L1L2-Gal4* driver in *ort* mutant flies restored their ‘on’- and ‘off’-transients.

(C) Real-time head yaw optomotor responses measured in wild-type (green) and *ort* mutants (red). Motion stimuli were provided by a striped drum rotating in alternate directions for 30 sec per direction (see Experimental Procedures for details). Wild-type flies responded to the rotating striped drum with syndirectional head turning while *ort* mutants exhibited no significant response. Means of responses were plotted (in degrees of rotation; 0°: initial head position; negative/positive: clockwise/counterclockwise rotation). Error bars (standard deviation): variations among 30 trials.

(D) Histogram of optomotor responses of wild-type and various *ort* mutants. *Ort*, but not *HisClI*, mutants exhibited essentially no optomotor response. Expressing Ort using the *ort^{Cl-4}-Gal4* or *L1L2-Gal4* driver rescued optomotor defects in *ort* mutants. Expressing *shi^{ts1}* using the *ort^{Cl-4}-Gal4* driver abolishes flies’ optomotor response at the restrictive, but not permissive, temperatures. Error bars indicate standard deviations.

Figure S5. Different Surface Receptors Label Distinct Medulla and Lobula Strata

(A-C) The expression patterns of three surface receptors, Fasciclin III (FasIII), Connectin (Con), and Capricious (Caps) in optic lobes examined by antibody labeling (magenta). (D-E) The antibodies against the presynaptic protein Bruchpilot (Brp/NC82) and postsynaptic marker Discs large (Dlg) were used to label the columnar and laminar structures of the optic lobes (magenta). Photoreceptor axons were labeled by MAb24B10 (white). Ort-expressing neurons were visualized using the *ort^{Cl-3}*-LexA::VP16 driver and the LexAop-rCD2::GFP reporter (green). The following antibodies were labeled (magenta).

(A-A'') Anti-FasIII immunolabeling.

(B-B'') Anti-Con immunolabeling.

(C-C'') Anti-Cap immunolabeling.

(D-D'') nc82 immunolabeling.

(E-E'') Anti-Dlg immunolabeling.

(A'-E', A''-E'') High magnification views of (A-E), respectively.

(A'''-E''') Green channel from Ort expressing neurons omitted from (A-E) to reveal the neuropil strata and photoreceptor terminals.

(F) Schematic representations of (A'''-E'''). Various saturation levels of magenta indicate the different expression levels of receptors and markers.

Scale bar: in (A), 20 μm for (A-E, A'''-E'''); in (A'), 10 μm for (A'-E', A''-E'').

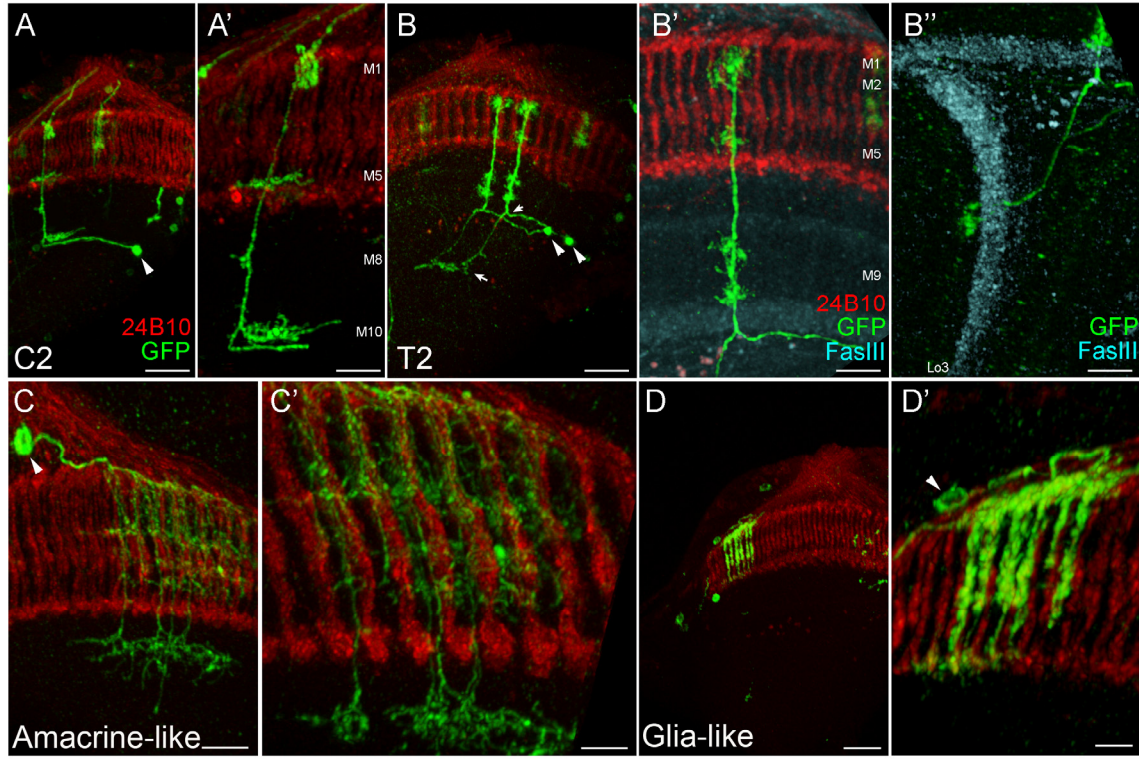


Figure S6. Ort Is Expressed in Centrifugal Neurons C2 and T2 as well as in Medulla Amacrine-Like and Glia-Like Cells

Single-neuron clones were generated using the flip-out mosaic system and labeled with the mCD8-GFP marker (green) as described in Figure 3. MAb24B10 (red) and anti-FasIII (cyan), labeling photoreceptors and specific strata respectively, serve as landmarks. The *ort^{Cl-3}-Gal4* driver was expressed in two types of centrifugal neurons, C2 (A, A') and T2 (B-B''), with cell bodies (arrowheads) located in the lobula plate cortex (see Figure 1A).

(A, A') The C2 neuron projects axons through the medulla neuropil and terminates at the lamina (not shown). Its axon arborizes in medulla strata M1, M5 and M10.

(B-B'') A pair of T2 neurons. Their axons bifurcate just beneath stratum M10 (small arrow): one branch terminates at lobula stratum Lo3 and the other arborizes at medulla strata M2, M5, and M9 and terminates at stratum M1.

The *ort^{Cl-3}-Gal4* driver also labeled at low frequency two novel medulla cells, designated amacrine-like and glia-like cells. The cell bodies are marked by arrowheads (C, D').

(C) The amacrine-like cell extends complex wide-field processes spanning multiple medulla columns.

(D) The glia-like cell has a soma in the cortex (arrowhead) and wraps around multiple columns containing photoreceptor terminals.

Scale Bar: in (A, B, D), 20 μm ; in (A', B', B''), 8 μm ; in (C), 10 μm ; in (C', D'), 5 μm .

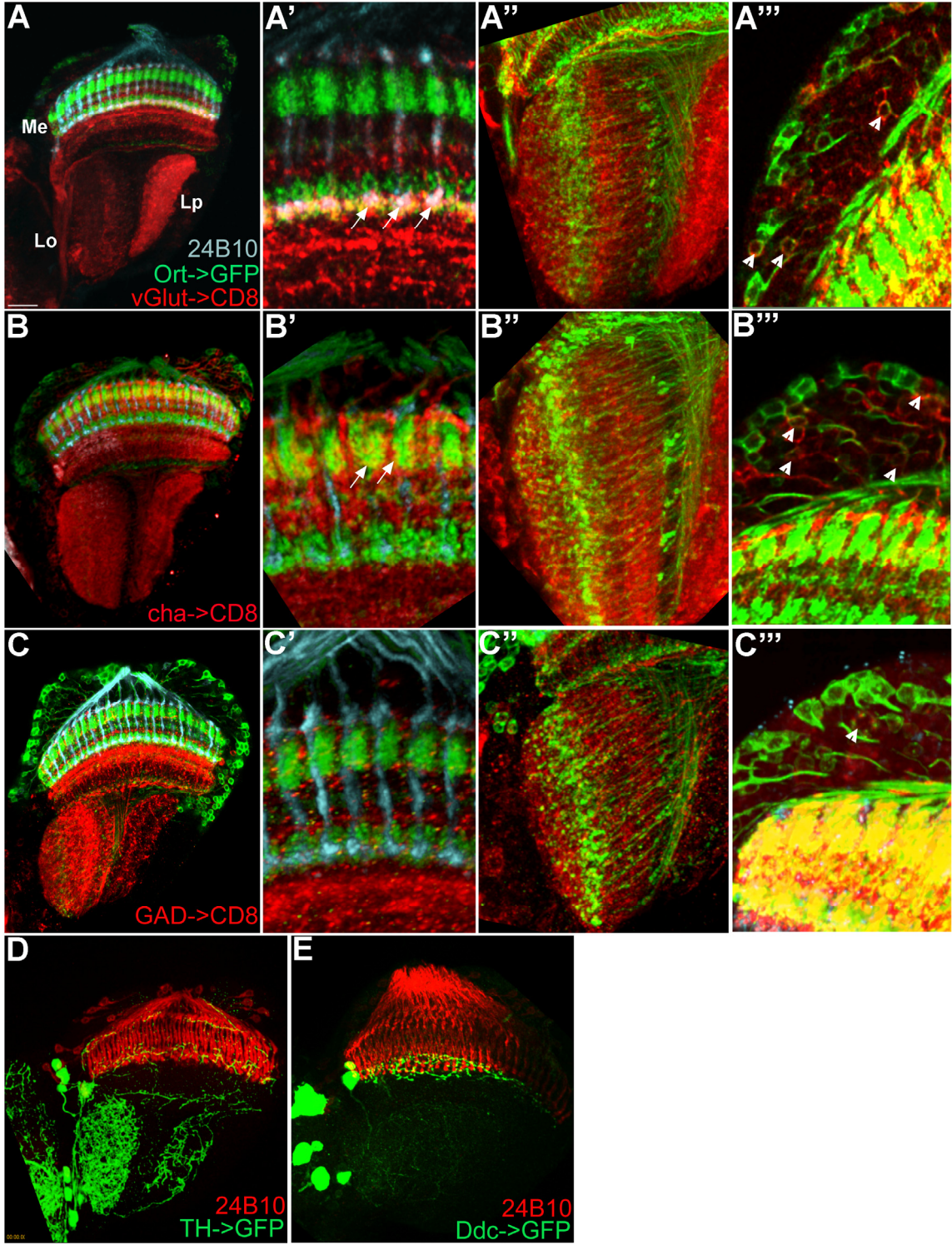


Figure S7. Neurotransmitter Phenotype of Ort-Expressing Neurons Assessed Using Gal4 Lines

Neurotransmitter contents in Ort-expressing neurons was examined using a dual-expression system. (A-C'') Ort-expressing neurons were labeled using *ort^{C1-3}-LexA::VP16* and *LexAop-rCD2::GFP* (green). Various Gal4 lines were used to express the CD8 marker (red) in neuron subsets that express different neurotransmitter phenotypes (see Experimental Procedures for details). Photoreceptor axons were labeled with MAb24B10 (cyan).

(A-A'') The expression pattern of *vGlut-Gal4* (vesicular glutamate transporter), a phenotypic marker for glutamatergic neurons. Note that there is significant overlap between GFP and CD8 labeling in medulla stratum M6 (arrows, A'), which was likely brought about by the processes of Dm8 neurons. A number of cell bodies in the medulla cortex was marked with both GFP and CD8 (arrowheads, A'').

(B-B'') The *cha-Gal4* (choline acetyltransferase) expression pattern, a phenotypic marker for cholinergic neurons. Note that GFP and CD8 signals co-localize to stratum M2 (arrows, B'), likely brought about by the axon terminals of L2 neurons.

(C-C'') The *GAD-Gal4* (glutamic acid decarboxylase I) expression pattern for GABAergic neurons. Minimal overlapping between GFP and CD8 labeling in the medulla neuropil (C') and cortex (C'') was found.

(D-E) Possible dopaminergic and serotonergic neurons were identified by using *TH-Gal4* and *Ddc-Gal4* to drive the expression of mCD8GFP marker (green). (D) The *TH-Gal4* (tyramine hydroxylase) expression pattern. (E) The *Ddc-Gal4* (DOPA decarboxylase) expression pattern. Both drivers labeled only tangential neurons in the medulla.

(A'-C'), (A''-C''), and (A'''-C'') are high magnification views of the medulla, lobula, and medulla cortex of (A-C), respectively. Scale bar: 20 μm in (A) for (A-E).

References

Friggi-Grelin, F., Coulom, H., Meller, M., Gomez, D., Hirsh, J., and Birman, S. (2003). Targeted gene expression in *Drosophila* dopaminergic cells using regulatory sequences from tyrosine hydroxylase. *J. Neurobiol.* 54, 618–627.

Hong, S.T., Bang, S., Paik, D., Kang, J., Hwang, S., Jeon, K., Chun, B., Hyun, S., Lee, Y., and Kim, J. (2006). Histamine and its receptors modulate temperature-preference behaviors in *Drosophila*. *J. Neurosci.* 26, 7245–7256.

Mahr, A., and Aberle, H. (2006). The expression pattern of the *Drosophila* vesicular glutamate transporter: a marker protein for motoneurons and glutamatergic centers in the brain. *Gene Expr. Patterns* 6, 299–309.

Ng, M., Roorda, R.D., Lima, S.Q., Zemelman, B.V., Morcillo, P., and Miesenbock, G. (2002). Transmission of olfactory information between three populations of neurons in the antennal lobe of the fly. *Neuron* 36, 463–474.

Sepp, K.J., and Auld, V.J. (1999). Conversion of lacZ enhancer trap lines to GAL4 lines using targeted transposition in *Drosophila melanogaster*. *Genetics* 151, 1093–1101.

Yasuyama, K., Kitamoto, T., and Salvaterra, P.M. (1995). Localization of choline acetyltransferase-expressing neurons in the larval visual system of *Drosophila melanogaster*. *Cell Tissue Res.* 282, 193–202.